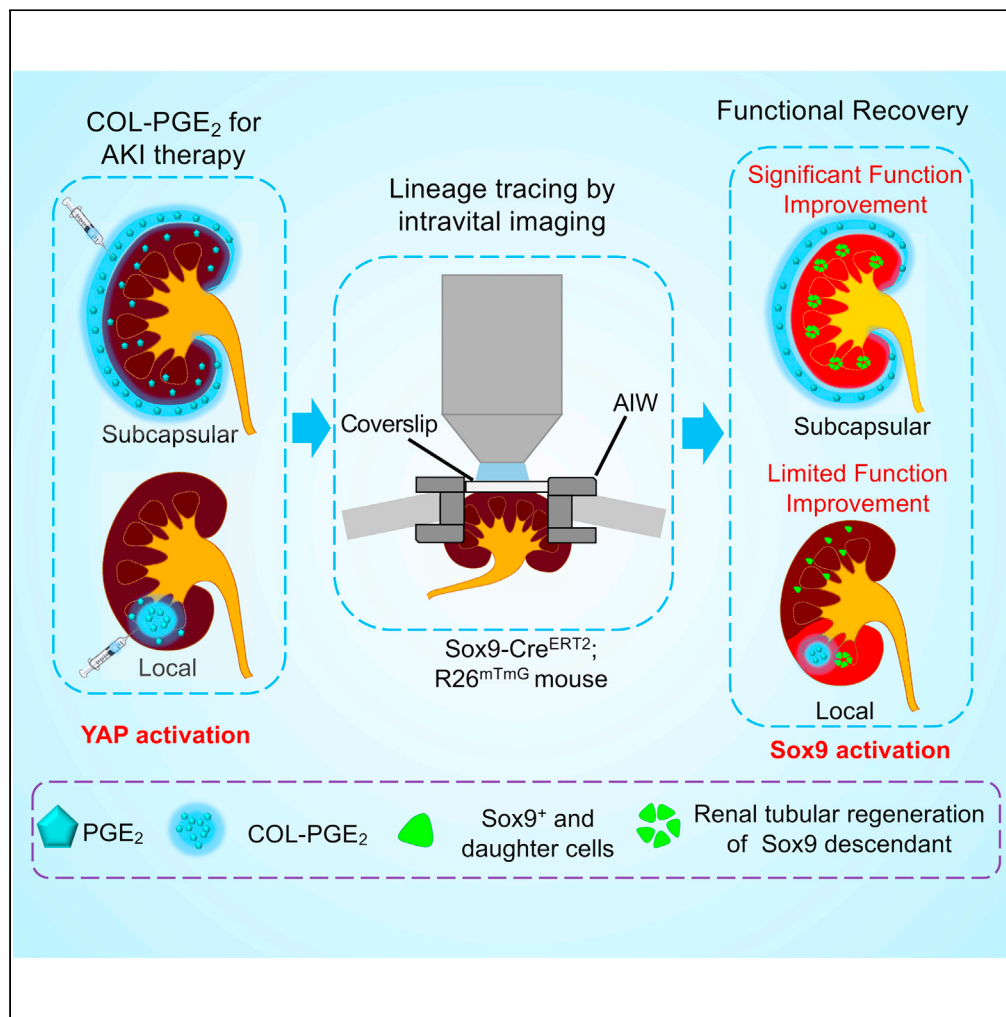


Article

# Renal subcapsular delivery of PGE<sub>2</sub> promotes kidney repair by activating endogenous Sox9<sup>+</sup> stem cells



Shang Chen,  
Haoyan Huang,  
Yue Liu, ..., Qiang  
Zhao, Xiang-Mei  
Chen, Zongjin Li

zongjinli@nankai.edu.cn (Z.L.)  
xmchen301@126.com (X.-  
M.C.)

**Highlights**

PGE<sub>2</sub> exhibits an adequate long-term release by being covalently cross-linked to collagen

The renal subcapsular space serves as a reservoir for the delivery of PGE<sub>2</sub>

Sox9<sup>+</sup> renal progenitor cells can be lineage traced intravitaly by microscopy

PGE<sub>2</sub> activates the endogenous renal progenitor Sox9<sup>+</sup> cells through the YAP pathway

Chen et al., iScience 24,  
103243  
November 19, 2021 © 2021  
The Author(s).  
[https://doi.org/10.1016/  
j.isci.2021.103243](https://doi.org/10.1016/j.isci.2021.103243)



## Article

Renal subcapsular delivery of PGE<sub>2</sub> promotes kidney repair by activating endogenous Sox9<sup>+</sup> stem cells

Shang Chen,<sup>1,2,9</sup> Haoyan Huang,<sup>1,2,9</sup> Yue Liu,<sup>1</sup> Chen Wang,<sup>1</sup> Xiaoniao Chen,<sup>3</sup> Yuqiao Chang,<sup>4</sup> Yuhao Li,<sup>1</sup> Zhikun Guo,<sup>4</sup> Zhibo Han,<sup>5,6</sup> Zhong-Chao Han,<sup>5,6,7</sup> Qiang Zhao,<sup>2</sup> Xiang-Mei Chen,<sup>8,\*</sup> and Zongjin Li<sup>1,2,4,8,10,\*</sup>

## SUMMARY

Prostaglandin E<sub>2</sub> (PGE<sub>2</sub>) has recently been recognized to play a role in immune regulation and tissue regeneration. However, the short half-life of PGE<sub>2</sub> limits its clinical application. Improving the delivery of PGE<sub>2</sub> specifically to the target organ with a prolonged release method is highly desirable. Taking advantage of the adequate space and proximity of the renal parenchyma, renal subcapsular delivery allows minimally invasive and effective delivery to the entire kidney. Here, we report that by covalently cross-linking it to a collagen matrix, PGE<sub>2</sub> exhibits an adequate long-term presence in the kidney with extensive intraparenchymal penetration through renal subcapsular delivery and significantly improves kidney function. Sox9 cell lineage tracing with intravital microscopy revealed that PGE<sub>2</sub> could activate the endogenous renal progenitor Sox9<sup>+</sup> cells through the Yap signaling pathway. Our results highlight the prospects of utilizing renal subcapsular-based drug delivery and facilitate new applications of PGE<sub>2</sub>-releasing matrices for regenerative therapy.

## INTRODUCTION

Acute kidney injury (AKI), which leads to abrupt loss of kidney function, is highly associated with the subsequent risks of chronic kidney disease and end-stage renal disease, which will lead to the need for lifelong dialysis and renal replacement therapy and cause high morbidity and mortality (James et al., 2020; Liu et al., 2020; Zhang et al., 2020; Zhang and Li, 2020). Methods for delivering stem cells, cytokines, and biomaterials to the kidney, such as systemic administration, intrarenal parenchyma injection, or intrarenal artery injection, offer promise for kidney regeneration after AKI (Fazekas and Griffin, 2020; Gao et al., 2020; Gonzalez et al., 2019; Little and Kairath, 2016). Targeting delivery specifically to the whole kidney, by which therapeutic drug levels can be maintained over time, is highly desirable. Local delivery results in high drug deposition and even toxic concentrations but leads to a dose that is lower than that required in more distant areas of the injected tissue. Intrarenal artery injection or systemic administration will also lead to poor local retention and insufficient distribution throughout the entire renal parenchyma over time (Segura-Ibarra et al., 2017). Renal subcapsular spaces under kidney capsules located on the surface of the kidneys have been widely used for cell or tissue transplantation because cells exhibit better growth in these spaces (Cunha and Baskin, 2016; van den Berg et al., 2018), and this provides insight into the use of subcapsular transplantation for AKI therapy to increase drug concentrations in the whole kidney (Dankers et al., 2015; Morizane and Bonventre, 2017; Segura-Ibarra et al., 2017).

Prostaglandin E<sub>2</sub> (PGE<sub>2</sub>), a kind of prostaglandin, has been recognized to play an important role in tissue regeneration and maintenance when the concentration of PGE<sub>2</sub> in injured tissues is elevated (Palla et al., 2021; Zhang et al., 2015). PGE<sub>2</sub> is synthesized by cyclooxygenase (COX) and prostaglandin E synthases (PGES) from arachidonic acid and interacts with four G-protein-coupled E-prostanoid receptors designated EP1, EP2, EP3, and EP4 to cause various downstream effects, including angiogenesis, inflammation, and stem cell development (Cheng et al., 2021; Norregaard et al., 2015; Zhang and Daaka, 2011). Recent studies revealed that injury-induced PGE<sub>2</sub> secretion is key to activating endogenous stem/progenitor cells for myocardial regeneration after infarction (FitzSimons et al., 2020; Hsueh et al., 2014). Moreover, PGE<sub>2</sub> shows obvious anti-inflammatory and pro-angiogenesis effects by inducing macrophage polarization from the M1 phenotype to the M2 phenotype at injured sites. In addition, PGE<sub>2</sub> in hepatocytes inhibits the activation of hepatic stellate cells and attenuates liver fibrosis in mice (Brea et al., 2018). Increasing

<sup>1</sup>School of Medicine, Nankai University, 94 Weijjin Road, Tianjin 300071, China

<sup>2</sup>The Key Laboratory of Bioactive Materials, Ministry of Education, Nankai University, The College of Life Sciences, Tianjin, China

<sup>3</sup>Beijing Tongren Eye Center, Beijing Tongren Hospital, Capital Medical University, Beijing, China

<sup>4</sup>Henan Key Laboratory of Medical Tissue Regeneration, Xinxiang Medical University, Xinxiang, China

<sup>5</sup>Jiangxi Engineering Research Center for Stem Cell, Shangrao, Jiangxi, China

<sup>6</sup>Tianjin Key Laboratory of Engineering Technologies for Cell Pharmaceutical, National Engineering Research Center for Cell Products, AmCellGene Co., Ltd., Tianjin China

<sup>7</sup>Beijing Engineering Laboratory of Perinatal Stem Cells, Beijing Institute of Health and Stem Cells, Health & Biotech Co., Beijing, China

<sup>8</sup>State Key Laboratory of Kidney Diseases, Chinese PLA General Hospital, 28 Fuxing Road, Beijing 100039, China

<sup>9</sup>Those authors contributed equally

<sup>10</sup>Lead contact

\*Correspondence: zongjinli@nankai.edu.cn (Z.L.), xmchen301@126.com (X.-M.C.)

<https://doi.org/10.1016/j.isci.2021.103243>



evidence revealed that PGE<sub>2</sub> is a promising therapeutic candidate for improving tissue repair and regeneration, reflected mainly in improving cutaneous wound healing, cardiac protection function, and accelerating liver regeneration (Chakkour and Kreydiyyeh, 2019; Xiao et al., 2004; Zhang et al., 2015, 2018). Furthermore, the main therapeutic mechanism of mesenchymal stem cells (MSCs) in tissue repair is mediated by the secretion of PGE<sub>2</sub> by MSCs (Cao et al., 2020; Du et al., 2016; Fazekas and Griffin, 2020; Zhang et al., 2018). However, the short half-life of PGE<sub>2</sub> *in vivo* limits its therapeutic efficiency in translational applications (Zhang et al., 2018). PGE<sub>2</sub> has a faster turnover rate of approximately 30 s in circulation due to degradation by 15-hydroxyprostaglandin dehydrogenase (15-PGDH), converting it into an inactivated 15-keto-PGE<sub>2</sub>, which limits its use to biomedical applications (Bygdeman, 2003; Kozak et al., 2001; Zhang et al., 2015). The strategy of conjugating PGE<sub>2</sub> by binding to biomaterials will maintain the presence of PGE<sub>2</sub> *in situ*, further enhancing the therapeutic effects of PGE<sub>2</sub> (Yao et al., 2015; Zhao et al., 2019). By facilitating the controlled release of PGE<sub>2</sub> *in situ*, renal subcapsular delivery provides a reservoir that allows the diffusion of PGE<sub>2</sub> into the entire kidney. Subcapsular delivery through sustained release of therapeutic drugs could avoid injury to the renal parenchyma and can result in maximal therapeutic efficacy in the kidney and minimal systemic side effects (Dankers et al., 2015).

Currently, it is believed that the kidney can regenerate itself after injury through dedifferentiation of tubular epithelial cells in the nephron or activation of resident/endogenous stem cells in the kidney (Zhang et al., 2020; Zhang and Li, 2020). However, the mechanisms of renal regeneration after AKI with or without treatment are poorly understood. Lineage tracing and two-photon intravital microscopy methods offer an opportunity to visualize cell behavior and examine dynamic cellular processes at the single-cell level in the context of intact organisms instead of in the *in vitro* environment (Boulch et al., 2019; Eles et al., 2019; Eng et al., 2018; Fan et al., 2018; Kaverina et al., 2019). Lineage tracing of kidney cells in living animals with intravital microscopy will unveil the potency and activities of renal resident cells after AKI (Liu and Li, 2021; Zhang and Li, 2020) and help to assess and determine the optimal therapeutics for AKI treatment. Sex-determining region Y box 9 (Sox9) has been shown to be a marker of renal progenitor cells that contributes to renal regeneration after AKI (Kang et al., 2016; Zhang and Li, 2020). To date, the therapeutic effect of PGE<sub>2</sub> through the promotion of Sox9<sup>+</sup> cell proliferation in AKI has not been investigated.

In addition, Hippo/Yap (Yes-associated protein) signaling pathway is composed of a series of conservative kinases, which mainly control organ size by regulating cell proliferation and apoptosis (Zhou et al., 2020). Specifically, the Yap signal controls genes that regulate cell and organism metabolism and coordinate organ growth and homeostasis with nutrition and metabolism (Moya and Halder, 2019). Several studies have revealed that activating Yap favors the regeneration of organs with poor or damaged regenerative capacity, such as the heart of adult mice (Li et al., 2020), the liver and intestines of elderly or diseased mice (Kim et al., 2017; Loforese et al., 2017), and injured skin (Moya and Halder, 2019). Limited, but convincing, evidence suggests that Yap plays an essential role in kidney and urinary tract development, podocyte homeostasis, fibrosis, and cystic and diabetic nephropathy (Chen et al., 2018; Wong et al., 2016).

The objective of this study was to investigate the potential use of the renal subcapsular space as a reservoir for the delivery of PGE<sub>2</sub> to the kidney. By covalently cross-linking it to a collagen matrix scaffold, we hypothesized that PGE<sub>2</sub> could significantly improve AKI via a site-specific, controlled-release drug delivery system. Furthermore, intravital microscopy was used to examine the spatiotemporal kinetics of kidney progenitor Sox9<sup>+</sup> cells under PGE<sub>2</sub> treatment using inducible Sox9 transgenic mice. Our results highlight the prospect of utilizing the renal subcapsular space for drug delivery for the treatment of kidney diseases. Furthermore, our data suggested that PGE<sub>2</sub> could promote renal regeneration by activating Sox9 through the Yap signaling pathway.

## RESULTS

### Synthesis and characterization of the COL-PGE<sub>2</sub> matrix

PGE<sub>2</sub> is rapidly metabolized *in vivo*, and the half-life of PGE<sub>2</sub> in the circulatory system is approximately 30 s (Bygdeman, 2003; Kozak et al., 2001; Zhang et al., 2018). To improve the therapeutic efficacy of PGE<sub>2</sub>, we developed a PGE<sub>2</sub> release matrix by cross-linking collagen type I with 4-hydrazinobenzoic acid (HBA)-polyethyleneimine (PEI), which was achieved by the reaction of the amine group on HBA with the carbonyl group on PGE<sub>2</sub> through condensation reactions (Figures 1A and S1A–S1C). The successful conjugation of HBA to PEI was confirmed by the appearance of carbonyl (C=O, ~1,651 cm<sup>-1</sup>) and N–N bond (~1,551 cm<sup>-1</sup>) vibrations in the Fourier transform infrared (FT-IR) spectroscopic analysis (Figure S2A).

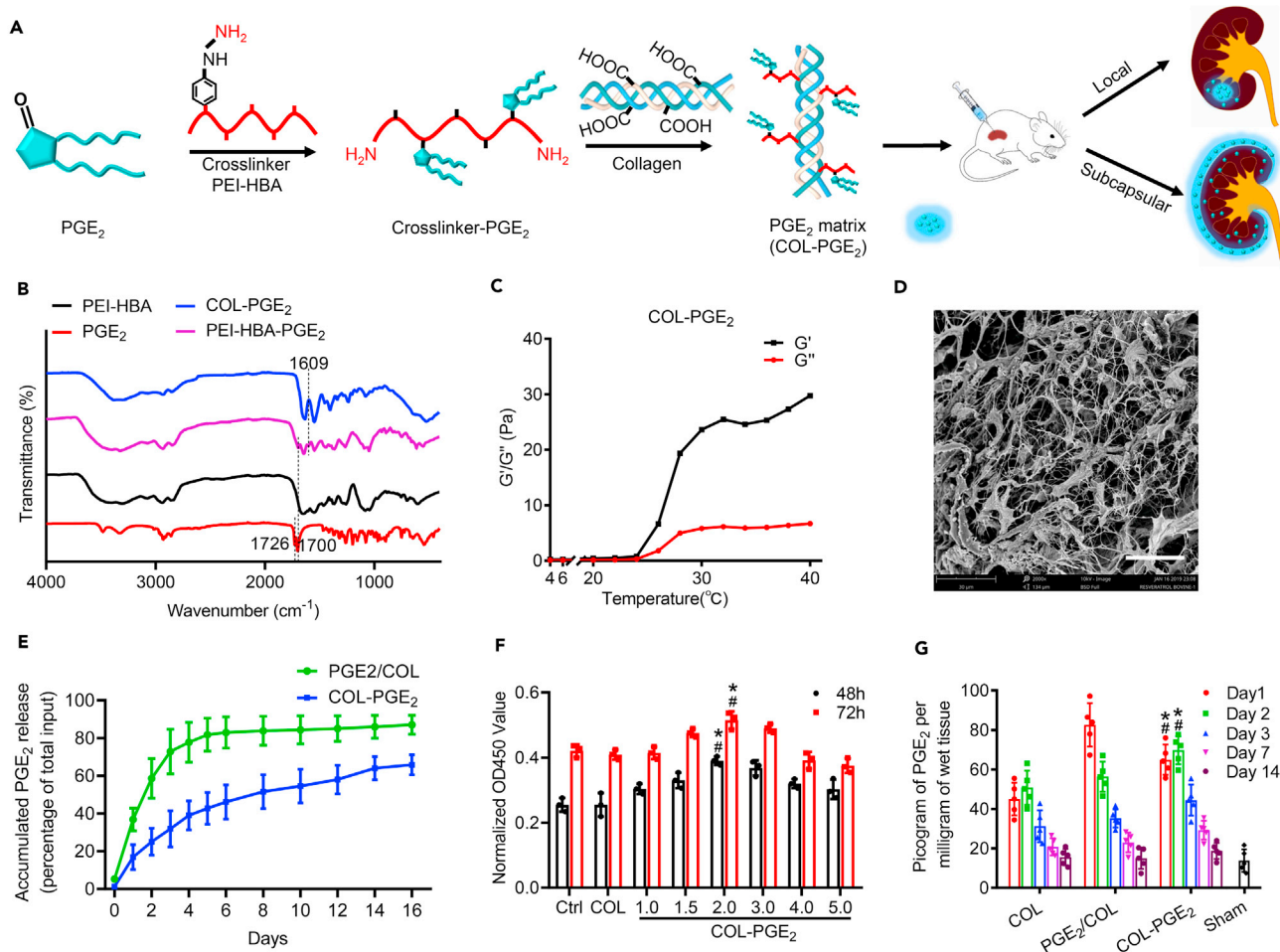


**Figure 1. Preparation and characterization of the COL-PGE<sub>2</sub> matrix**

(A) A schematic depicting the method of synthesis of the COL-PGE<sub>2</sub> matrix.  
 (B) FT-IR analysis shows the characteristic peaks of the PGE<sub>2</sub>, PEI (polyethyleneimine)-HBA (4-hydrazinobenzoic acid), PEI-HBA-PGE<sub>2</sub>, and COL-PGE<sub>2</sub> matrix. A peak at 1,609 cm<sup>-1</sup> revealed the successful conjugation of PGE<sub>2</sub>.  
 (C) Evaluation of the rheological profile of the COL-PGE<sub>2</sub> matrix by analyzing the storage modulus (G') and the loss modulus (G'') with temperature changes, which indicated the phase transition of the COL-PGE<sub>2</sub> matrix from a solution to a gel. Pa, pascal (unit of pressure or stress).  
 (D) Scanning electron micrograph image that reveals the morphologic structure of the lyophilized COL-PGE<sub>2</sub> matrix. Scale bars, 30 μm.  
 (E) *In vitro* release of PGE<sub>2</sub> by the COL-PGE<sub>2</sub> matrix. The COL-PGE<sub>2</sub> matrix was deposited in a test tube and covered with a layer of 1 × PBS buffer. The amount of released PGE<sub>2</sub> was determined by ELISA. Two-way repeated measures ANOVA with Sidak's post hoc test was used for statistical analysis. Data are expressed as mean ± SD; n = 3. The mixture of free PGE<sub>2</sub> with collagen was tested as a control, and the differences were significant between the COL-PGE<sub>2</sub> matrix (COL-PGE<sub>2</sub>) and the physical mix of free PGE<sub>2</sub> physical mix with collagen type I (PGE<sub>2</sub>/COL) from day 1 to day 16.  
 (F) CCK-8 assay showing proliferation of primary renal tubular epithelial cells with different concentrations of the COL-PGE<sub>2</sub> matrix. Two-way multivariate analysis of variance (two-way MANOVA) with the Tukey post hoc test was used for statistical analysis. Data are expressed as mean ± SD; n = 3, \*p < 0.05 versus COL; #p < 0.05 versus control.  
 (G) For *in vivo* PGE<sub>2</sub> release, COL, PGE<sub>2</sub>/COL, and COL-PGE<sub>2</sub> matrices were injected into the renal capsule of C57BL/6 mice after AKI. The kidney was then explanted by removing the kidney capsule and matrix at the indicated time points for the assessment of the released PGE<sub>2</sub> by ELISA. The concentration of PGE<sub>2</sub> in the kidney remains at high level from day 1 to day 3 and lasts for more than two weeks in the COL-PGE<sub>2</sub> group. Furthermore, PGE<sub>2</sub> can be found in normal tissue (Sham group), and injury (COL group) can stimulate PGE<sub>2</sub> secretion, but PGE<sub>2</sub> is at a low level. Two-way MANOVA with the Tukey post hoc test was used for statistical analysis. Data are expressed as mean ± SD; n = 5, \*p < 0.05 versus COL; #p < 0.05 versus PGE<sub>2</sub>/COL.

FT-IR spectroscopic analysis revealed the successful conjugation of PGE<sub>2</sub>, as revealed by the presence of a peak at 1,609 cm<sup>-1</sup>, confirming the presence of the C=N bond in the structure, whereas the band at 1,700 cm<sup>-1</sup> corresponded to the C=O bonds in the carboxyl groups of PGE<sub>2</sub>. Furthermore, the carbonyl (~1,726 cm<sup>-1</sup>) vibrations of PGE<sub>2</sub> disappeared in the spectra of PEI-HBA-PGE<sub>2</sub>, demonstrating that hydrazone bonds were formed and that no free PGE<sub>2</sub> existed in addition to PEI-HBA-PGE<sub>2</sub> (Figure 1B). Then, the

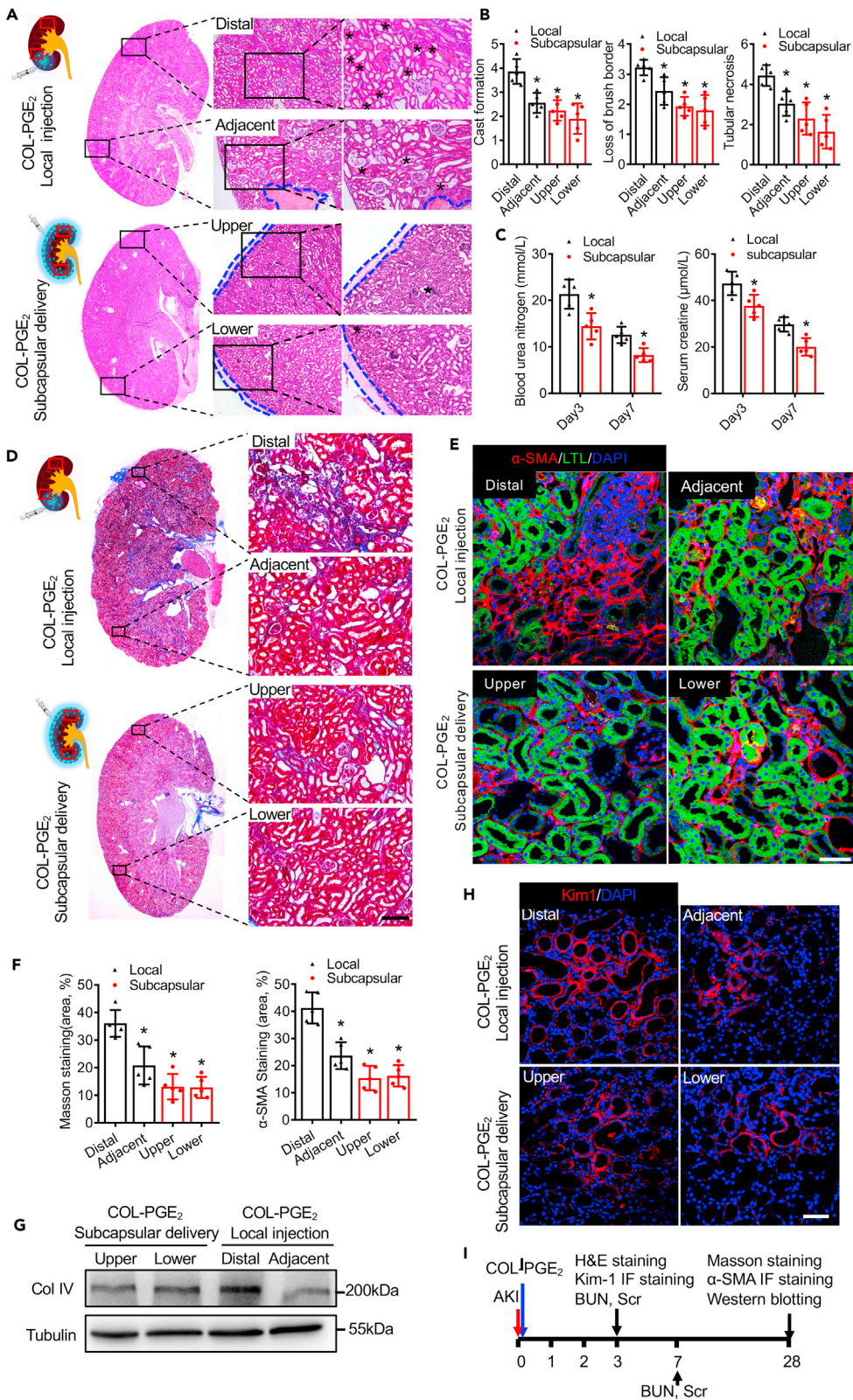


**Figure 2. Subcapsular delivery of the COL-PGE<sub>2</sub> matrix is superior to local injection in kidney recovery**

(A) Histological analysis of kidney injury by H&E staining on day 3 post-AKI. Top: COL-PGE<sub>2</sub> matrix local injection; bottom: COL-PGE<sub>2</sub> matrix subcapsular delivery. Massive necrosis is observed in proximal tubules with hyaline casts (asterisks), and subcapsular delivery of the COL-PGE<sub>2</sub> matrix is superior to local injection for kidney recovery. The blue dotted lines indicate the edges of the COL-PGE<sub>2</sub> matrix. Rectangles in schema represent Distal, Adjacent (upper panel) and Upper, Lower (lower panel), respectively. Scale bars, 100  $\mu$ m.

(B) Quantification of typical pathological changes, such as cast formation, tubular necrosis, and loss of the brush border.

(C) Serum blood levels of urea nitrogen (left) and creatinine (right) were measured at different time points after AKI.

(D) Representative images of kidney sections stained with Masson trichrome stain on day 28 after AKI. Rectangles in the schema represent Distal, Adjacent (upper panel) and Upper, Lower (lower panel), respectively. Scale bars, 100  $\mu$ m.

(E) Representative images of  $\alpha$ -SMA (red) immunofluorescence staining on day 28 after AKI. The proximal tubules were co-stained with Lotus Tetragonolobus Lectin (LTL; green). Scale bars, 50  $\mu$ m.

(F) Quantitative analysis of Masson trichrome staining (left) and the  $\alpha$ -SMA<sup>+</sup> staining area (right) were performed to evaluate renal fibrosis.

(G) Immunoblot analysis of type IV collagen (Col IV) protein in the kidney on day 28 after AKI.

(H) Representative images of Kim-1 (red) immunofluorescence staining on day 3 after AKI. Scale bars, 50  $\mu$ m.

(I) Schematics of the time lines for each experiment. One-way repeated measures ANOVA with Tukey post hoc tests (B, C, and G) was used for statistical analysis. Data are expressed as mean  $\pm$  SD; n = 5, \*p < 0.05 versus distal positions of the local injection of the COL-PGE<sub>2</sub> matrix local injection.

PEI-HBA-PGE<sub>2</sub> conjugates were further cross-linked to collagen by dehydration (Figure S1C). The extent of cross-linking was further confirmed by tris-borate-EDTA-PAGE, an electrophoresis technique optimized to detect free PEI-HBA-PGE<sub>2</sub>. Prior to ultrafiltration, only traces of free PEI-HBA-PGE<sub>2</sub> were detected, indicating a high degree of cross-linking (Figure S2B). The PGE<sub>2</sub> loading capacity of the COL-PGE<sub>2</sub> matrix was 1.78 micrograms of PGE<sub>2</sub> per milligram of collagen, as quantified by ELISA (Figure S2C).

Rheological methods were used to analyze the gelation properties of the matrix of PGE<sub>2</sub>-conjugated collagen (COL-PGE<sub>2</sub> matrix). The rheological profile showing the temperature changes of the COL-PGE<sub>2</sub> matrix was evaluated and compared with that of the collagen matrix without immobilization of PGE<sub>2</sub> (Figure S2D). With an increase in temperature from 4°C to 40°C, the storage modulus (G') of the COL-PGE<sub>2</sub> matrix showed obvious enhancement, indicating the phase transition from a solution to a gel (Figure 1C). The gelation temperature of the COL-PGE<sub>2</sub> matrix was between 26°C and 27°C, which was similar to that of the collagen matrix and free PGE<sub>2</sub> in the collagen matrix, indicating that the COL-PGE<sub>2</sub> matrix could transform from a liquid to a gel at body temperature *in situ*. The morphological structure of the lyophilized COL-PGE<sub>2</sub> matrix was observed by scanning electron microscopy (SEM). The matrix showed homogeneous and interconnected protein filaments, the average width of which was approximately 5  $\mu$ m (Figure 1D), which was similar to that of collagen or free PGE<sub>2</sub> in the collagen matrix (Figure S2E).

To test whether the COL-PGE<sub>2</sub> matrix results in the release of PGE<sub>2</sub>, we investigated the release kinetics of the COL-PGE<sub>2</sub> matrix and free PGE<sub>2</sub> in collagen by ELISA. Free PGE<sub>2</sub> in collagen was rapidly released within the first two to three days, whereas the COL-PGE<sub>2</sub> matrix demonstrated prolonged release that lasted more than 16 days *in vitro* (Figure 1E). To investigate the PGE<sub>2</sub> release curve of the COL-PGE<sub>2</sub> matrix *in vitro*, a CCK-8 assay was used to determine the optimal concentration (2  $\mu$ M) of the COL-PGE<sub>2</sub> matrix that can noticeably promote cell proliferation (Figure 1F). The *in vivo* release of PGE<sub>2</sub> from the COL-PGE<sub>2</sub> matrix showed that the level of PGE<sub>2</sub> increased incrementally after injection, whereas unbound PGE<sub>2</sub> was released rapidly in the first 3 days (Figure 1G).

**Subcapsular delivery of the COL-PGE<sub>2</sub> matrix exerts superior therapeutic effects**

Local delivery results in a high level of drug deposition and poor local retention (Segura-Ibarra et al., 2017). To determine the therapeutic efficacy of renal subcapsular delivery, we investigated the therapeutic efficacy of the COL-PGE<sub>2</sub> matrix in a mouse AKI model. First, the results of histological examination showed that necrotic tubule and hyaline cast were significantly reduced by subcapsular delivery compared with local injection of the COL-PGE<sub>2</sub> matrix. Specifically, subcapsular delivery of the COL-PGE<sub>2</sub> matrix significantly reduced the damage caused by AKI throughout the entire kidney, whereas local injection of the COL-PGE<sub>2</sub> matrix only repaired renal tissue near the injection site (adjacent), and locations further away from the injection sites (distal) still showed severe damage (Figures 2A and 2B). Additionally, to assess functional recovery after AKI, blood urea nitrogen (BUN) and serum creatinine (Scr) were detected on day 3 and 7. We found that subcapsular delivery of the COL-PGE<sub>2</sub> matrix accelerated kidney functional recovery compared with local injection, as shown by the lower values of BUN and Scr (Figure 2C).

During the later phase of kidney injury, renal fibrosis generally leads to progressive dysfunction, which can ultimately result in end-stage renal disease (Feng et al., 2016; Zhang et al., 2020). Therefore, we performed Masson trichrome staining and anti- $\alpha$ -Smooth muscle actin ( $\alpha$ -SMA) immunostaining to assess renal fibrosis on day 28 after AKI. Quantification of the fibrotic area showed that subcapsular delivery of the COL-PGE<sub>2</sub> matrix significantly alleviated renal fibrosis in the entire kidney compared with local injection (Figures 2D and 2F). Anti- $\alpha$ -SMA immunostaining also confirmed that subcapsular delivery of the COL-PGE<sub>2</sub> matrix could alleviate renal fibrosis (Figures 2E and 2F). In addition, the histological results were further confirmed by western blotting analysis of collagen type IV (a marker of fibrosis) (Figure 2G). Furthermore, the evaluation of a kidney injury marker (Kim-1) by immunostaining revealed consistent results (Figure 2H). Schematics of the time lines for each experiment are shown in Figure 2I. In conclusion, compared with local injection, subcapsular delivery of the COL-PGE<sub>2</sub> matrix exhibited superior outcomes in improving renal function by attenuating renal injury and suppressing renal fibrosis. Meanwhile, these results also proved the feasibility of subcapsular delivery of the COL-PGE<sub>2</sub> matrix for kidney therapy.

### PGE<sub>2</sub> promotes kidney repair through Yap-mediated activation of Sox9

Based on the great repair effect of PGE<sub>2</sub> on the injured kidney, we investigated the therapeutic mechanism of the COL-PGE<sub>2</sub> matrix in AKI. Our results confirmed that PGE<sub>2</sub> could promote cell proliferation by Ki-67 staining (Figures S3A and S3B). Sox9 is a key factor in kidney regeneration (Kang et al., 2016; Zhang and Li, 2020). Interestingly, its upstream regulator, Yap, also plays an important role during animal development and regeneration (Chen et al., 2018; Moya and Halder, 2019). To explore the potential role of their interaction in kidney repair, in the present study, the western blotting analysis results showed that the COL-PGE<sub>2</sub> matrix significantly increased the expression of Yap and downstream targets of amphiregulin (Areg, an EGFR ligand, promotes epithelial regeneration) (Chen et al., 2018; Zaiss et al., 2015), Survivin (an antiapoptotic molecule in renal cells) (Chen et al., 2013; Kindt et al., 2008), and Sox9. Large tumor suppressor kinase 1 (Lats1) is the major negative regulator of Yap, which sequesters Yap in the cytoplasm by phosphorylating it at the Ser127 residue. However, PGE<sub>2</sub> did not affect the ratio of phosphorylated Yap. In addition, PGE<sub>2</sub> did not affect Lats1 phosphorylation of Lats1 (Figure S3C). Furthermore, we investigated the relationship between Yap and Sox9 activity, and a positive correlation between Yap and Sox9 activity was observed in the group treated with the COL-PGE<sub>2</sub> matrix (Figures S3D and S3E).

In addition, compared with subcapsular delivery of the COL-PGE<sub>2</sub> matrix, local injection resulted in an increase in Ki-67<sup>+</sup> cells near the injection site, but this beneficial effect was not observed throughout the kidney (Figures 3A and 3C). Furthermore, subcapsular delivery increased the expression of Yap and its target genes Areg, Survivin, and Sox9 throughout the entire kidney, whereas local injection of the COL-PGE<sub>2</sub> matrix only increased its expression in the location near the injected site (Figures 3B–3D). These results indicated that the therapeutic contributions of the COL-PGE<sub>2</sub> matrix to renal repair include stimulation of endogenous cell proliferation and anti-apoptosis through Yap-mediated Sox9 activation.

### Enhanced therapeutic effects of the PGE<sub>2</sub>-releasing matrix

We confirmed that renal subcapsular delivery of the COL-PGE<sub>2</sub> matrix exhibited a greater advantage in improving renal function compared with local injection. To test whether sustained release improved the therapeutic efficacy of PGE<sub>2</sub>, a murine model of AKI was applied. We delivered PBS, collagen type I (COL), free PGE<sub>2</sub> with collagen type I (PGE<sub>2</sub>/COL), and COL-PGE<sub>2</sub> matrix (PGE<sub>2</sub>-conjugated collagen matrix) through the renal capsule. Histological changes in the early stage (day 3 post-AKI) were evaluated by hematoxylin and eosin (H&E) staining. Massive tubular cell necrosis and hyaline cast formation were observed in the proximal tubules of the kidneys in the PBS group, whereas these pathological phenomena were significantly less common in the COL-PGE<sub>2</sub> matrix group (Figures 4A and 4B). Next, we evaluated the expression of Kim-1 by immunostaining. Compared with the other three groups (PBS, COL, and PGE<sub>2</sub>/COL), the group treated with the COL-PGE<sub>2</sub> matrix showed fewer Kim-1<sup>+</sup> renal tubules on day 3 post-AKI (Figures S4A and S4B). In addition, BUN and Scr were measured on day 3 and 7 post-AKI to assess renal function. The increasing concentrations of BUN and Scr reflected the deterioration of renal function. Administration of the COL-PGE<sub>2</sub> matrix markedly improved renal function compared with the other three groups, manifested as a reduction in BUN and Scr levels (Figure 4C). Masson trichrome staining demonstrated a significant reduction in fibrotic area in the COL-PGE<sub>2</sub> matrix group compared with the other groups (Figures 4D and 4F).  $\alpha$ -SMA staining also demonstrated findings similar to Masson trichrome staining (Figures 4E and 4F). Furthermore, histological results were supported by a type IV collagen western blot analysis (Figure 4G). Furthermore, we evaluated the degradation and safety of the COL-PGE<sub>2</sub> matrix in the

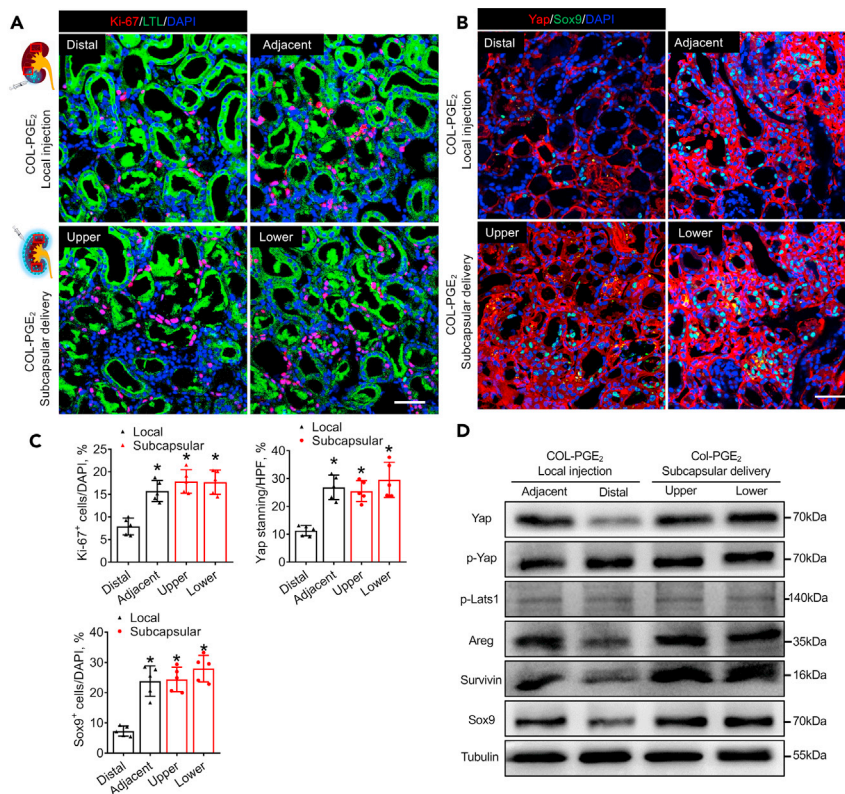


**Figure 3. Subcapsular delivery of the COL-PGE<sub>2</sub> matrix stimulates Yap-mediated expression of Sox9 in the whole kidney**

(A) Representative images show Ki-67 immunostaining (red) detected in renal tubular epithelial cells (FITC-labeled LTL, green) 3 days after injury. Rectangles in the schema represent Distal, Adjacent (upper panel) and Upper, Lower (lower panel), respectively. Scale bars, 50  $\mu$ m.

(B) Immunofluorescence staining of Yap and Sox9 in renal tubular epithelial cells on day 3 after AKI with subcapsular/local delivery of the COL-PGE<sub>2</sub> matrix. Scale bars, 50  $\mu$ m.

(C) Quantitative analysis of the immunostaining of Ki-67, Yap, and Sox9 immunostaining.

(D) Immunoblotting analysis of the Yap, p-Yap, p-Lats1, Areg, Survivin, and Sox9 protein in kidneys treated with subcapsular/local injection of the COL-PGE<sub>2</sub> matrix on day 3 after AKI. One-way repeated measures ANOVA with Tukey post hoc tests (C) was used for statistical analysis. Data are expressed as mean  $\pm$  SD; n = 5, \*p < 0.05 versus distal positions of the local injection of the COL-PGE<sub>2</sub> matrix local injection. HPF, high-power field.

kidney, and the COL-PGE<sub>2</sub> matrix was almost completely degraded after 28 days (Figures S4C and S4D). H&E staining was also performed; there were no pathological changes in the heart, liver, spleen, and lung in each group after treatment with the COL, PGE<sub>2</sub>/COL, and COL-PGE<sub>2</sub> matrix on day 28 after AKI (Figure S4E). Schematics of the time lines for each experiment are revealed in Figure 4H. In conclusion, the COL-PGE<sub>2</sub> matrix was superior in promoting kidney regeneration by gradually releasing PGE<sub>2</sub>.

### Lineage tracing of Sox9<sup>+</sup> cells by intravital microscopy after COL-PGE<sub>2</sub> matrix therapy

High-resolution intravital two-photon microscopy (TPM) offers a platform for investigating the spatiotemporal kinetics of endogenous stem cells in tissue regeneration at the single-cell level (Dondossola et al., 2018; Hato et al., 2017; Honkura et al., 2018; Zhang and Li, 2020). Recent evidence indicates that Sox9<sup>+</sup> cells show progenitor-like properties and that proliferation and differentiation of Sox9<sup>+</sup> endogenous renal progenitor cells are mainly responsible for renal tubular regeneration after AKI (Kang et al., 2016; Kumar et al., 2015). In this study, a mouse model of the Sox9 lineage tracing (Balani et al., 2017; Roche et al., 2015; Zhang and Li, 2020; Zhang et al., 2016), Sox9-Cre<sup>ERT2</sup>; R26<sup>mTmG</sup>, was used to monitor Sox9<sup>+</sup> cells and their descendants with an abdominal imaging window (AIW) (Figures 5A–5C). Furthermore, we performed intravital lineage tracing of Sox9<sup>+</sup> cells in AKI mice (Figure 5B). The results revealed that EGFP was only expressed

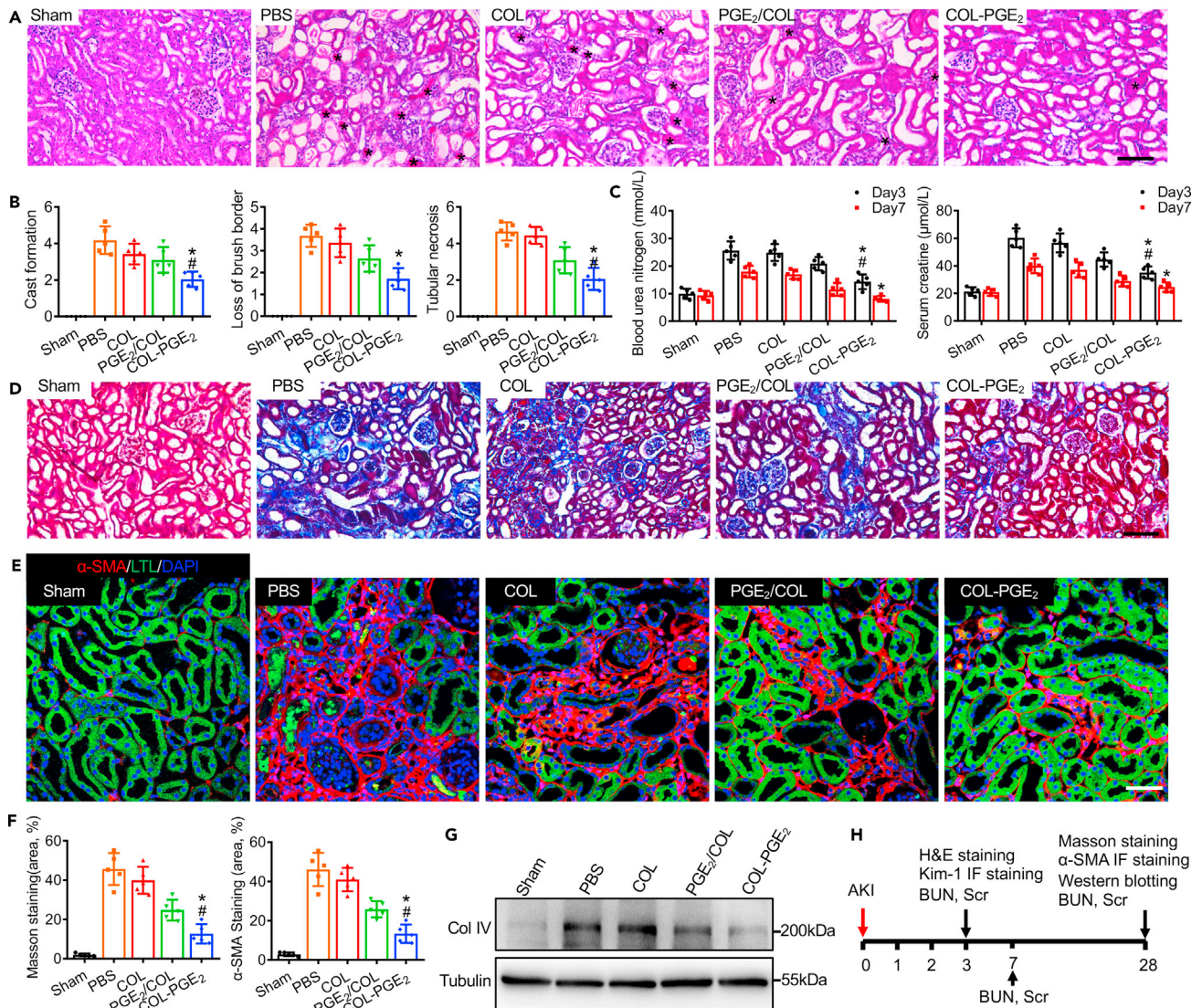


**Figure 4. The COL-PGE<sub>2</sub> matrix attenuates renal fibrosis and accelerates renal recovery**

(A) Representative images of the histological analysis of kidney injury by H&E staining on day 3 after treatment with the PBS, COL, PGE<sub>2</sub>/COL, and COL-PGE<sub>2</sub> matrices after AKI. Massive necrosis was observed in the proximal tubules with hyaline casts (asterisks), and subcapsular delivery of the COL-PGE<sub>2</sub> matrix revealed to have almost complete prevention of histopathological alterations after AKI. Scale bars, 100  $\mu$ m.

(B) Quantitative evaluations of cast formation, tubular necrosis, and injured tubules.

(C) Serum blood levels of urea nitrogen (left) and creatinine (right) were measured at different time points after AKI.

(D) Representative images of Masson trichrome staining of renal tissues harvested on day 28 after AKI. Scale bars, 100  $\mu$ m.

(E) Representative images of anti- $\alpha$ -SMA immunostaining (red) of renal tissues harvested on day 28 after AKI. Proximal tubules were co-stained with FITC-labeled LTL (green). Scale bars, 50  $\mu$ m.

(F) Quantitative analysis of Masson trichrome staining (left) and the  $\alpha$ -SMA<sup>+</sup> staining area (right) was performed to evaluate renal fibrosis.

(G) Immunoblotting analysis of type IV collagen (Col IV) in the kidney on day 28 after AKI.

(H) Schematics of the time lines for each experiment. One-way repeated measures ANOVA with Tukey post hoc tests (B, C, and F) was used for statistical analysis. Data are expressed as mean  $\pm$  SD; n = 5, \*p < 0.05 versus COL; #p < 0.05 versus PGE<sub>2</sub>/COL.

in Sox9<sup>+</sup> cells after tamoxifen induction and that there was no spontaneous AKI-induced Cre activation in Sox9-Cre<sup>ERT2</sup>; R26<sup>mTmG</sup> mice (Figure S5).

Our results revealed that Sox9<sup>+</sup> cells can be tracked with intravital TPM and that the COL-PGE<sub>2</sub> matrix significantly increased the number of EGFP<sup>+</sup> cells, which can form renal tubular structures on day 7 after

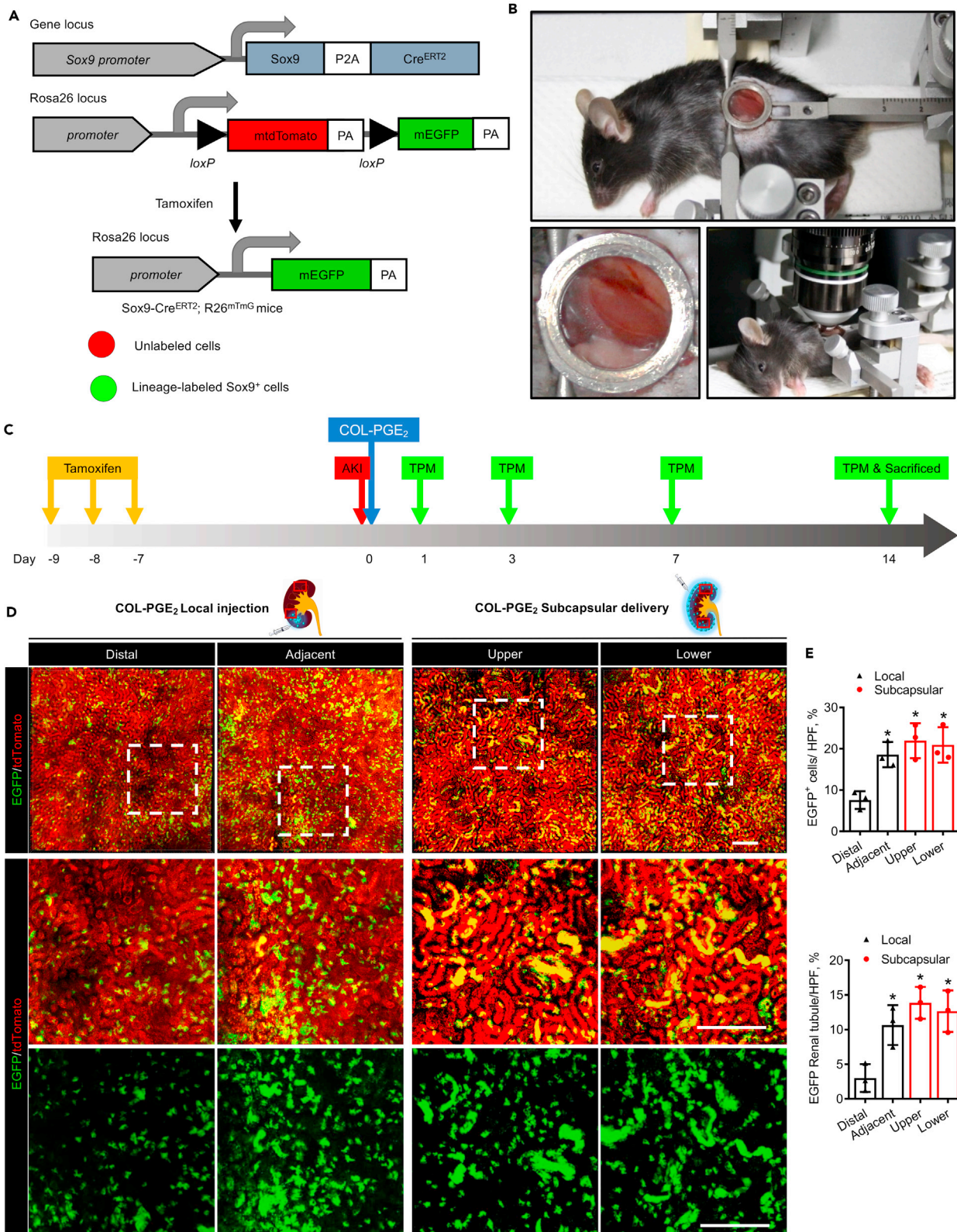


**Figure 5. Sox9<sup>+</sup> cell expansion under COL-PGE<sub>2</sub> matrix therapy by intravital microscopy**

(A) Scheme of the generation of tamoxifen-inducible Sox9-Cre<sup>ERT2</sup>; R26<sup>mTmG</sup> mice for genetic lineage tracing. Polyadenylation sequences (PA).  
 (B) Sox9-Cre<sup>ERT2</sup>; R26<sup>mTmG</sup> mouse with the abdominal imaging window (AIW) on the left kidney (top). Close-up view of the kidney window (left). Mouse with AIW installed for two-photon intravital microscopy analysis (right).  
 (C) Schematic illustration of two-photon live cell imaging of Sox9<sup>+</sup> cells after AKI and COL-PGE<sub>2</sub> matrix administration. Sox9-Cre<sup>ERT2</sup>; R26<sup>mTmG</sup> mice were injected intraperitoneally with tamoxifen once a day for three continuous days to label Sox9<sup>+</sup> cells. Seven days after the final tamoxifen injection, renal ischemia-reperfusion injury was induced in these mice with simultaneous implantation of AIW. Two-photon intravital microscopy imaging was performed on days 1, 3, 7, and 14 after AKI.  
 (D) Representative images of two-photon intravital tracing showed that Sox9<sup>+</sup>-cell-derived cells expanded abundantly after subcapsular delivery of the COL-PGE<sub>2</sub> matrix compared with local injection on day 7 after AKI. Rectangles in the schema represent Distal, Adjacent (upper panel) and Upper, Lower (lower panel), respectively. Scale bar, 200 μm.  
 (E) Quantification of EGFP-labeled renal tubules and Sox9<sup>+</sup>/EGFP co-labeled cells in the kidneys of mice on day 7 with subcapsular/local delivery of the COL-PGE<sub>2</sub> matrix post-AKI. One-way repeated measures ANOVA with Tukey post hoc tests were used for statistical analysis. Data are expressed as mean ± SD; n = 3, \*p < 0.05 versus distal positions of COL-PGE<sub>2</sub> matrix local injection. See also [Videos S5, S6, S7, and S8](#).

AKI ([Figure S6](#)). In the sham operation group, all renal cells were substantially positive for tdTomato, indicating that renal cells were largely Sox9<sup>-</sup> in the normal adult kidney. Compared with local injection, subcapsular delivery of the COL-PGE<sub>2</sub> matrix increased the number of EGFP<sup>+</sup> cells in the entire kidney and led to the obvious formation of renal tubular structures ([Figure 5D](#) and [Videos S5, S6, S7, and S8](#)). Furthermore, subcapsular delivery of the COL-PGE<sub>2</sub> matrix promoted the expansion of EGFP<sup>+</sup> cells throughout the entire kidney, whereas local injection increased the expansion only near the injected site ([Figures 5E and S7; Videos S1, S2, S3, S4, S5, S6, S7, and S8](#)).

To investigate Sox9 activity under the treatment of the COL-PGE<sub>2</sub> matrix, we further performed an anti-Sox9 immunostaining analysis of kidney samples collected from Sox9-Cre<sup>ERT2</sup>; R26<sup>mTmG</sup> mice on day 14 after the last round of TPM imaging. In normal adult kidneys, EGFP<sup>+</sup> cells were rare, and most of the cells were Sox9<sup>-</sup> ([Figure S8](#)); this suggested that only a small fraction of renal cells was derived from Sox9<sup>+</sup> cells under physiological conditions. Post-AKI, renal injury promoted Sox9 expression and stimulated the expansion of EGFP<sup>+</sup> cells, but most descendants of EGFP<sup>+</sup> cells no longer expressed Sox9. It was intriguing that the COL-PGE<sub>2</sub> matrix promoted the expansion of EGFP<sup>+</sup> cells and maintained their expression of Sox9 for a period of time ([Figures 6A, 6B, and 6E](#)). Additionally, subcapsular delivery of the COL-PGE<sub>2</sub> matrix stimulated Sox9 expression and cell proliferation (Ki-67) compared with local injection ([Figures 6C–6E](#)). Taken together, these findings indicated that the COL-PGE<sub>2</sub> matrix promoted the expansion of EGFP<sup>+</sup> cells while maintaining their progenitor cell characteristics and stimulated more cells to express Sox9 after enhancing their proliferation capacity. The COL-PGE<sub>2</sub> matrix also boosted the formation of functional renal tubules by promoting the proliferation of Sox9<sup>+</sup> cell descendants.

**Cytoprotective effects of the COL-PGE<sub>2</sub> matrix**

To verify the mechanism of the PGE<sub>2</sub> matrix in kidney repair, we isolated primary renal tubular epithelial cells (pRTECs) from C57BL/6 mice, which were confirmed by cell morphology and immunofluorescence staining of E-cadherin and Aquaporin-1 ([Figures S9A and S9B](#)). The morphology and colony-forming capacity of pRTEC and trypan blue stain revealed the superior biocompatibility of the COL-PGE<sub>2</sub> matrix ([Figures S9C and S9D](#)). Immunofluorescence results showed that the expression of the proliferation-related gene Ki-67 was drastically upregulated in pRTEC cultured on COL-PGE<sub>2</sub>-matrix-coated plates compared with that in pRTECs cultured on PGE<sub>2</sub>/COL-matrix-coated, COL-matrix-coated, or noncoated plates ([Figure 7A](#)). To examine the cell protective effects of the COL-PGE<sub>2</sub> matrix, pRTECs were cultured in plates coated with COL, PGE<sub>2</sub>/COL, and COL-PGE<sub>2</sub> matrix and treated with hydrogen peroxide (H<sub>2</sub>O<sub>2</sub>). Staining of apoptotic cells with Hoechst 33,342 demonstrated that the PGE<sub>2</sub>/COL and COL-PGE<sub>2</sub> matrix significantly reduced the apoptosis of pRTECs induced by H<sub>2</sub>O<sub>2</sub> ([Figure S10](#)). To determine the pathway involved in this protective action, we measured the expression of genes in pRTEC after treatment with H<sub>2</sub>O<sub>2</sub> (150 μM) for 6 h. Treatment with H<sub>2</sub>O<sub>2</sub> increased the expression of the apoptosis-associated genes Bad, Bax, Caspase-3, and Fas in pRTEC. Coating plates with the PGE<sub>2</sub>/COL and COL-PGE<sub>2</sub> matrix significantly reduced the expression of these genes ([Figure 7B](#)). Additionally, the COL-PGE<sub>2</sub> matrix stimulated pRTEC proliferation and survival of pRTECs through the Yap-mediated Areg and Survivin pathway and promoted the activation of Sox9, a marker of renal progenitor cell ([Figures 7C–7E](#)). Unlike the activation of Yap by the COL-PGE<sub>2</sub> matrix, PGE<sub>2</sub> failed to activate Sox9 in pRTEC with Yap depletion. Furthermore, depletion of Yap by shRNA resulted in a reduction of Areg and Survivin, even though pRTECs were treated with the COL-PGE<sub>2</sub>

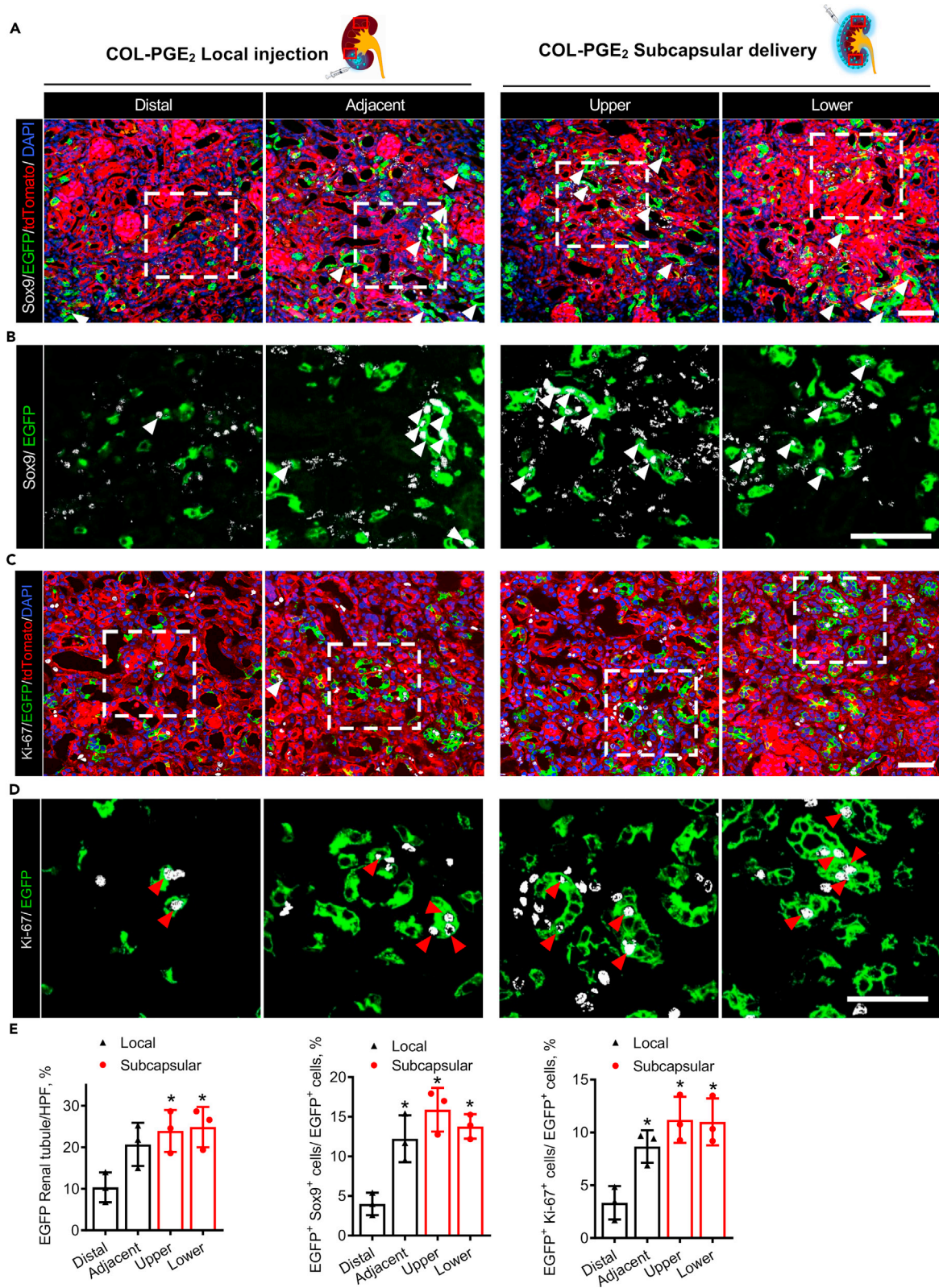


**Figure 6. Subcapsular delivery of the COL-PGE<sub>2</sub> matrix results in greater activation of Sox9 expression and Sox9<sup>+</sup> cell proliferation**

(A and B) (A) Confocal images and (B) local zoomed-in images for colocalization analysis of anti-Sox9 immunostaining (gray) and Sox9-Cre<sup>ERT2</sup>-activated EGFP fluorescence in kidneys with local injection (left) and subcapsular delivery (right) of the COL-PGE<sub>2</sub> matrix on day 14 post-AKI. White arrowheads highlight the renal tubules formed by Sox9-EGFP-labeled cells, and white arrowheads highlight Sox9<sup>+</sup>/EGFP co-labeled cells. Rectangles in the schema represent Distal, Adjacent (upper panel) and Upper, Lower (lower panel), respectively. Scale bar, 50 μm.  
(C and D) (C) Confocal images and (D) local magnification images for colocalization analysis of anti-Ki-67 immunostaining (gray) and Sox9-Cre<sup>ERT2</sup>-activated EGFP fluorescence in kidneys with local injection (left) and subcapsular delivery (right) of the COL-PGE<sub>2</sub> matrix on day 14 post-AKI. Red arrowheads highlight Ki-67<sup>+</sup>/EGFP<sup>+</sup> co-labeled cells. Scale bar, 50 μm.  
(E) Quantification of EGFP<sup>+</sup> renal tubules, Sox9<sup>+</sup>/EGFP<sup>+</sup> co-labeled cells, and Ki-67<sup>+</sup>/EGFP<sup>+</sup> co-labeled cells in the kidneys of mice on day 14 after subcapsular or local delivery of the COL-PGE<sub>2</sub> matrix post-AKI. One-way repeated measures ANOVA with Tukey post hoc tests (E) was used for statistical analysis. Data are expressed as mean ± SD; n = 3, \*p < 0.05 versus distal positions of the local injection of the COL-PGE<sub>2</sub> matrix local injection.

matrix (Figures 7F–7H). In conclusion, the COL-PGE<sub>2</sub> matrix favors the proliferation of renal tubular epithelial cells and exerts cytoprotective effects *in vitro*.

## DISCUSSION

This study demonstrates that renal subcapsular delivery of the COL-PGE<sub>2</sub> matrix effectively improves functional recovery after AKI. The COL-PGE<sub>2</sub> matrix results in an adequate long-term release of PGE<sub>2</sub> in the kidney with extensive intraparenchymal penetration and maintenance of PGE<sub>2</sub> release. This approach overcomes the limitations of conventional local free drug delivery, which cannot provide sustained drug release for long periods and results in insufficient distribution within the whole kidney. Sox9 cell lineage tracing with intravital microscopy revealed that PGE<sub>2</sub> could significantly ameliorate kidney function by activating the renal endogenous progenitor Sox9<sup>+</sup> cells through the Yap signaling pathway. We highlight the potential of COL-PGE<sub>2</sub> matrix administration in the perirenal space as a viable strategy for local and sustained delivery in kidney disease therapy.

PGE<sub>2</sub> has long been recognized to play a role in immune regulation and tissue regeneration (Martinez-Collon and Moore, 2018; Nasrallah et al., 2016; Palla et al., 2021). However, its short half-life time *in vivo* limits the application of PGE<sub>2</sub>. Several strategies, such as inhibition of the PGE<sub>2</sub> catabolizing enzyme, covalent coupling of PGE<sub>2</sub> with prodrugs, or incorporation of PGE<sub>2</sub> into biomaterials to prolong release, have been applied in regenerating therapy (Young and Grynepas, 2018; Zhang et al., 2015, 2018). To our knowledge, this is the first study of immobilization of PGE<sub>2</sub> within a collagen matrix for endogenous progenitor activation. Slow release of bioactive small molecules through covalent coupling to the matrix is an attractive strategy to enhance tissue regeneration after injury or damage and to ensure safety and effectiveness. Our findings highlight the potential use of the COL-PGE<sub>2</sub> matrix as a novel therapeutic strategy to promote renal tissue regeneration through subcapsular transplantation.

Previous investigations have shown that administering drugs in the peri-organ space of organs such as the heart and kidney provides a strategy to utilize a site-specific prolonged drug release reservoir to target organs at high local concentrations (Garcia et al., 2017; Segura-Ibarra et al., 2017; Soranno et al., 2016). The unique space of the perirenal sac makes it an ideal platform for drug elution on the surface of the kidney, avoiding tissue damage by local injection and a lack of drug distribution to positions farther away from injection sites. Our results reveal the drawback of local PGE<sub>2</sub> delivery, which leads to limited improvement in renal function. Covalent cross-linking of growth factors, peptides, or small molecules with biomaterials, such as collagen matrix, polymers, dendrimers, and chitosan scaffolds, produces an injectable and stabilized matrix for the delivery of pro-survival factor in tissue injury therapy (Feng et al., 2016; Lee et al., 2018; Zhang and Li, 2020; Zhao et al., 2019). In this study, an injectable PGE<sub>2</sub> collagen matrix was generated by cross-linking collagen with PGE<sub>2</sub> through polyethyleneimine (PEI). Furthermore, the hydrazone bond formed between PGE<sub>2</sub> and PEI is an unstable covalent bond, and the collagen matrix will serve as a reservoir of PGE<sub>2</sub> for prolonged release. In summary, we have demonstrated the safety and feasibility of our renal capsular delivery method according to the standards of the Food and Drug Administration and have shown that it is compatible with PGE<sub>2</sub> and collagen, providing an example of its translational application to AKI therapy.

Stem cell therapy holds great promise for kidney regeneration after AKI (Fazekas and Griffin, 2020; Feng et al., 2016; James et al., 2020; Zaw Thin et al., 2020). However, acute cell death, immune responses, oncogenic properties, and ethical concerns limit the use of stem cells in clinical practice (Choumerianou et al., 2008), and few such therapies have succeeded in clinical practice (Lumelsky et al., 2018). The strategy based

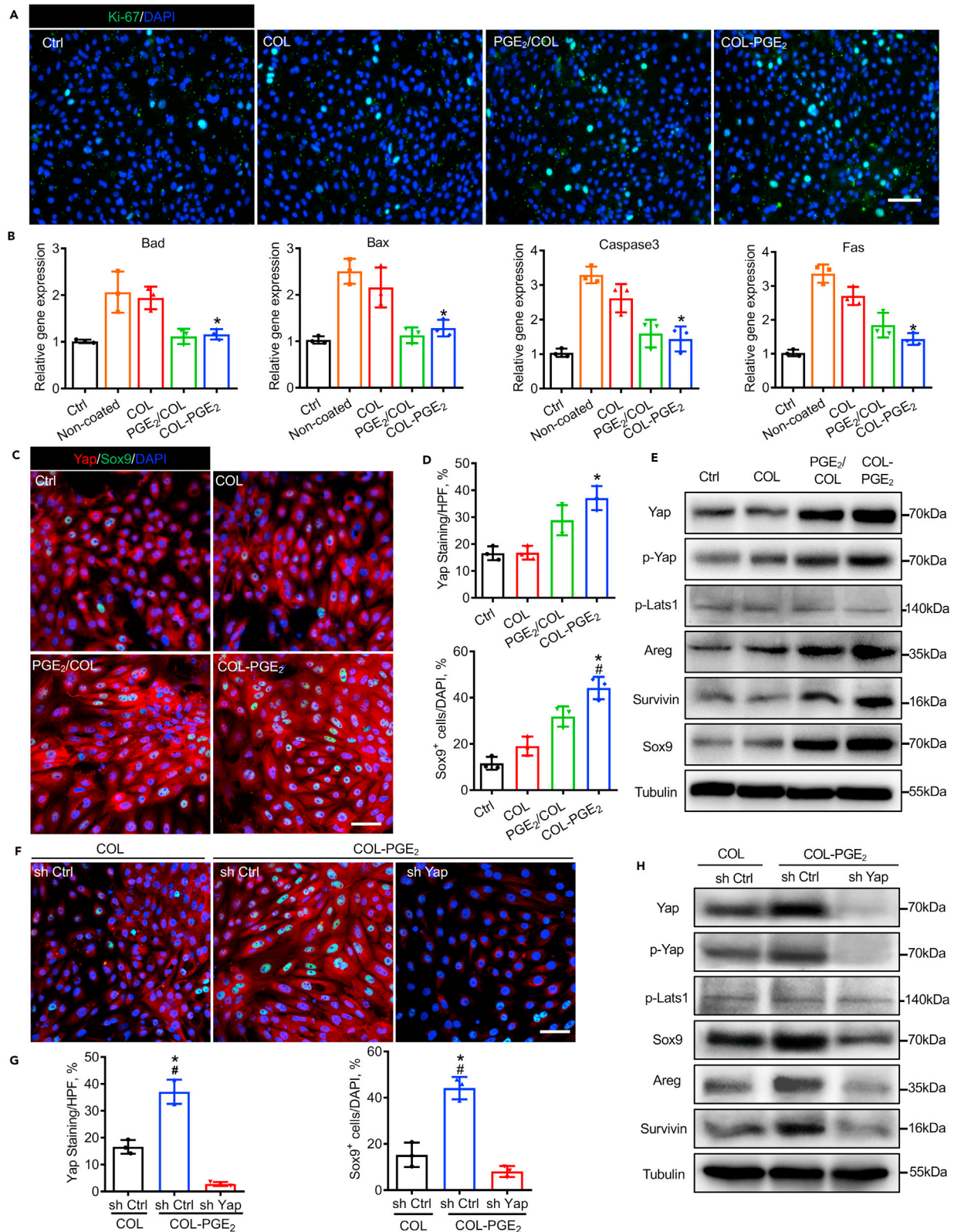


**Figure 7. The COL-PGE<sub>2</sub> matrix favors renal tubular epithelial cell proliferation and cytoprotection *in vitro***

(A) Immunofluorescence staining of Ki-67 (green) in primary renal tubular epithelial cells (pRTECs) cultured on plates coated with 2.0 μM COL-PGE<sub>2</sub>, PGE<sub>2</sub>/COL, or COL matrix or uncoated plates. Scale bars, 100 μm.  
 (B) Expression levels of apoptosis-related genes were evaluated by qPCR.  
 (C) Immunofluorescence staining of Yap (red) and Sox9 (green) in pRTEC cultured in noncoated, COL, PGE<sub>2</sub>/COL, or COL-PGE<sub>2</sub> at 48 h. Scale bars, 50 μm.  
 (D) Quantification of the Yap<sup>+</sup> area and Sox9<sup>+</sup> cells in (C).  
 (E) Immunoblot analysis of the Yap, p-Yap, p-Lats1, Areg, Survivin, and Sox9 protein in pRTEC cultured on noncoated, COL, PGE<sub>2</sub>/COL, or COL-PGE<sub>2</sub> matrix at 48 h. β-tubulin was used as loading control.  
 (F) Immunofluorescence staining of Yap (red) and Sox9 (green) in pRTEC cultured in plates coated with COL or COL-PGE<sub>2</sub> and pRTECs with YAP knockdown cultured on plates at 48 h. Scale bars, 50 μm.  
 (G) Quantification of the Yap<sup>+</sup> area and Sox9<sup>+</sup> cells in (F).  
 (H) Western blot analysis of the Yap, p-Yap, p-Lats1, Areg, Survivin, and Sox9 protein in pRTEC cultured on COL- or COL-PGE<sub>2</sub>-coated plates and pRTEC with Yap knockdown cultured on plates at 48 h. β-tubulin was used as loading control. One-way repeated measures ANOVA with Tukey post hoc tests (B and D) was used for statistical analysis. Data are expressed as mean ± SD; n = 3. \*p < 0.05 versus COL; #p < 0.05 versus PGE<sub>2</sub>/COL. One-way repeated measures ANOVA with Tukey post hoc tests (G) was used for statistical analysis. Data are expressed as mean ± SD; n = 3. \*p < 0.05 versus the non-targeting shRNA (sh Ctrl) cultured in COL; #p < 0.05 versus the shRNA targeting YAP (sh-Yap) cultured in COL-PGE<sub>2</sub>.

on optimizing endogenous tissue responses and activation of resident stem cells will enhance tissue healing and regeneration (Lumelsky et al., 2018; Tremblay et al., 2020). Tissue-resident stem cells in specific microenvironments are tightly regulated by extrinsic and intrinsic factors of cells for tissue homeostasis and regeneration (He et al., 2014; Liu et al., 2016; Lumelsky et al., 2018). Targeting the repair pathway by activating endogenous stem cells will offer a framework for AKI therapy (Humphreys et al., 2016; Zhang et al., 2020; Zhang and Li, 2020). Sox9<sup>+</sup> cells have been identified as endogenous renal progenitor cells, and studies indicate that proliferation and differentiation of Sox9<sup>+</sup> cells are primarily responsible for renal tubular regeneration and renal repair after AKI (Kang et al., 2016; Kumar et al., 2015). Yap activation has been shown to play an important role in renal repair after injury (Moya and Halder, 2019; Xu et al., 2016). Yap regulates the transcription of Sox9 through a conserved TEAD binding site in the Sox9<sup>+</sup> promoter (Song et al., 2014). We found that the COL-PGE<sub>2</sub> matrix could promote the proliferation of endogenous Sox9 progenitor cells by increasing the expression of the Yap protein and the number of Sox9<sup>+</sup> cells. Our results highlight that PGE<sub>2</sub> could activate endogenous Sox9<sup>+</sup> renal stem cells and reveal a potential therapeutic approach for AKI therapy. Advances in imaging-based monitoring methods have allowed the tracking of stem cells and the evaluation of their therapeutic effects (Huang et al., 2015; Liu et al., 2020; Zhang and Li, 2020). Intravital two-photon microscopy (TPM) with an abdominal imaging window (AIW) allows monitoring of the spatiotemporal dynamics of endogenous stem cells in the processes of tissue repair at the single-cell level in living animals longitudinally for weeks using a lineage tracing animal model (Hato et al., 2017; Rakhilin et al., 2019; Zhang and Li, 2020). In this study, Sox9<sup>+</sup> cell tracking provided new insights into the dynamic cellular processes involved in kidney regeneration with high resolution under treatment with the COL-PGE<sub>2</sub> matrix. Intravital lineage tracing offers a novel strategy for exploring the therapeutic mechanism of resident cells in tissue regeneration of the kidney and other organs.

In summary, we developed a novel method to deliver the PGE<sub>2</sub>-releasing matrix to the kidney through the perirenal sac. Many types of gel can be used with this platform, provide a new treatment strategy for kidney diseases, and may be particularly useful for the delivery of small molecular drugs, peptides, cytokines, miRNAs, and stem cells. By taking advantage of the adequate space and proximity of the renal parenchyma, renal subcapsular delivery is a minimally invasive and effective delivery technique for the entire kidney that will aid in the translation of drug-releasing biomaterials into the clinic for kidney diseases. Furthermore, the activation of endogenous Sox9<sup>+</sup> cells by PGE<sub>2</sub> with the lineage tracking method and intravital microscopy highlights the therapeutic effects of PGE<sub>2</sub> on tissue regeneration. Future studies are needed to better understand the underlying mechanisms of PGE<sub>2</sub> and optimize the COL-PGE<sub>2</sub> matrix system to help develop new methods for regenerative therapy. Overall, our study of the COL-PGE<sub>2</sub> matrix established a proof-of-concept for a therapeutic that is feasible and effective in improving AKI by activating resident stem cells of the kidney.

**Limitations of the study**

Renal subcapsular delivery presents many advantages over existing drug delivery methods that will aid in the translation of drug-releasing biomaterials into the clinic for kidney diseases. The application of subcapsular injection in clinical treatment still needs to explore more suitable methods for transplantation. In addition, PGE<sub>2</sub> activates the differentiation of endogenous Sox9<sup>+</sup> cells differentiation into renal tubular

epithelial cells and other kidney cells and is critically involved in kidney repair. However, it is not clear about the specific differentiation direction and tendency of Sox9<sup>+</sup> cells after PGE<sub>2</sub> treatment. Thus, more work is needed to understand how PGE<sub>2</sub>-induced Yap regulates the specific differentiation of Sox9<sup>+</sup> cells and which patients could benefit from Sox9 activation.

## STAR★METHODS

Detailed methods are provided in the online version of this paper and include the following:

- KEY RESOURCES TABLE
- RESOURCE AVAILABILITY
  - Lead contact
  - Materials availability
  - Data and code availability
- EXPERIMENTAL MODEL AND SUBJECT DETAILS
  - AKI model and COL-PGE<sub>2</sub> matrix delivery
  - Tracing of the Sox9 lineage with transgenic mice
- METHOD DETAILS
  - Preparation of the COL-PGE<sub>2</sub> matrix
  - Characterization of the COL-PGE<sub>2</sub> matrix
  - Biocompatibility of the COL-PGE<sub>2</sub> matrix
  - Measurement of PGE<sub>2</sub> release
  - Cell apoptosis assay
  - Knockdown of Yap in primary renal tubular epithelial cells
  - Intravital two-photon imaging in mice
  - Renal function analysis
  - Histological analysis of renal tissues
  - Western blot analysis
  - Quantitative real-time PCR
- QUANTIFICATION AND STATISTICAL ANALYSIS
- ADDITIONAL RESOURCES

## SUPPLEMENTAL INFORMATION

Supplemental information can be found online at <https://doi.org/10.1016/j.isci.2021.103243>.

## ACKNOWLEDGMENTS

This research was partially supported by National Key R&D Program of China (2017YFA0103200), National Natural Science Foundation of China (U2004126), and Postdoctoral Innovative Talent 799 Support Foundation (BX20190382).

## AUTHOR CONTRIBUTIONS

Z.L. and X.C. designed the experiments; S.C. and H. H. performed the experiments and analyzed the results; C. W. and Y. L. validated the results; X. C. and Y. C. performed cell experiments; Y. L. and H. H. bred and identified the transgenic animals; Z. L., S.C., and H. H. wrote the original draft preparation; Z.L., Z.G., and Z. H. reviewed and edited the manuscript; Z.L., X.C., Z.C.H., and Q.Z. edited the manuscript. All authors have read and agreed to the published version of the manuscript.

## DECLARATION OF INTERESTS

The authors declare no competing interests.

Received: June 18, 2021

Revised: August 19, 2021

Accepted: October 5, 2021

Published: November 19, 2021

## REFERENCES

- Balani, D.H., Ono, N., and Kronenberg, H.M. (2017). Parathyroid hormone regulates fates of murine osteoblast precursors in vivo. *J. Clin. Invest.* 127, 3327–3338. <https://doi.org/10.1172/JCI91699>.
- Boulch, M., Grandjean, C.L., Cazaux, M., and Bouso, P. (2019). Tumor immunosurveillance and immunotherapies: a fresh look from intravital imaging. *Trends Immunol.* 40, 1022–1034. <https://doi.org/10.1016/j.it.2019.09.002>.
- Brea, R., Motino, O., Frances, D., Garcia-Monzon, C., Vargas, J., Fernandez-Velasco, M., Bosca, L., Casado, M., Martin-Sanz, P., and Agra, N. (2018). PGE2 induces apoptosis of hepatic stellate cells and attenuates liver fibrosis in mice by downregulating miR-23a-5p and miR-28a-5p. *Biochim. Biophys. Acta Mol. Basis Dis.* 1864, 325–337. <https://doi.org/10.1016/j.bbadis.2017.11.001>.
- Bygdeman, M. (2003). Pharmacokinetics of prostaglandins. *Best Pract. Res. Clin. Obstet. Gynaecol.* 17, 707–716. [https://doi.org/10.1016/s1521-6934\(03\)00043-9](https://doi.org/10.1016/s1521-6934(03)00043-9).
- Cao, X., Duan, L., Hou, H., Liu, Y., Chen, S., Zhang, S., Liu, Y., Wang, C., Qi, X., Liu, N., et al. (2020). IGF-1C hydrogel improves the therapeutic effects of MSCs on colitis in mice through PGE2-mediated M2 macrophage polarization. *Theranostics* 10, 7697–7709. <https://doi.org/10.7150/thno.45434>.
- Chakkour, M., and Kreydiyyeh, S. (2019). FTY720P upregulates the Na<sup>+</sup>/K<sup>+</sup> ATPase in HepG2 cells by activating S1PR3 and inducing PGE2 release. *Cell Physiol. Biochem.* 53, 518–531. <https://doi.org/10.33594/000000155>.
- Chen, J., Chen, J.K., Conway, E.M., and Harris, R.C. (2013). Survivin mediates renal proximal tubule recovery from AKI. *J. Am. Soc. Nephrol.* 24, 2023–2033. <https://doi.org/10.1681/ASN.2013010076>.
- Chen, J., You, H., Li, Y., Xu, Y., He, Q., and Harris, R.C. (2018). EGF receptor-dependent YAP activation is important for renal recovery from AKI. *J. Am. Soc. Nephrol.* 29, 2372–2385. <https://doi.org/10.1681/ASN.2017121272>.
- Cheng, H., Huang, H., Guo, Z., Chang, Y., and Li, Z. (2021). Role of prostaglandin E2 in tissue repair and regeneration. *Theranostics* 11, 8836–8854. <https://doi.org/10.7150/thno.63396>.
- Choumerianou, D.M., Dimitriou, H., and Kalmanti, M. (2008). Stem cells: promises versus limitations. *Tissue Eng. Part B Rev.* 14, 53–60. <https://doi.org/10.1089/teb.2007.0216>.
- Cunha, G.R., and Baskin, L. (2016). Use of sub-renal capsule transplantation in developmental biology. *Differentiation* 91, 4–9. <https://doi.org/10.1016/j.diff.2015.10.007>.
- Dankers, P.Y.W., van Luyn, M.J.A., Huizinga-van der Vlag, A., Petersen, A.H., Koerts, J.A., Bosman, A.W., and Popa, E.R. (2015). Convenient formulation and application of a supramolecular ureido-pyrimidinone modified poly(ethylene glycol) carrier for intrarenal growth factor delivery. *Eur. Polym. J.* 72, 484–493. <https://doi.org/10.1016/j.eurpolymj.2015.07.010>.
- Dondossola, E., Alexander, S., Holzapfel, B.M., Filippini, S., Starbuck, M.W., Hoffman, R.M., Navone, N., De-Juan-Pardo, E.M., Logothetis, C.J., Hutmacher, D.W., and Friedl, P. (2018). Intravital microscopy of osteolytic progression and therapy response of cancer lesions in the bone. *Sci. Transl. Med.* 10. <https://doi.org/10.1126/scitranslmed.aao5726>.
- Du, W., Li, X., Chi, Y., Ma, F., Li, Z., Yang, S., Song, B., Cui, J., Ma, T., Li, J., et al. (2016). VCAM-1(+) placental chorionic villi-derived mesenchymal stem cells display potent pro-angiogenic activity. *Stem Cell Res. Ther.* 7, 49. <https://doi.org/10.1186/s13287-016-0297-0>.
- Eles, J.R., Vazquez, A.L., Kozai, T.D.Y., and Cui, X.T. (2019). Meningeal inflammatory response and fibrous tissue remodeling around intracortical implants: an in vivo two-photon imaging study. *Biomaterials* 195, 111–123. <https://doi.org/10.1016/j.biomaterials.2018.12.031>.
- Eng, D.G., Kaverina, N.V., Schneider, R.R.S., Freedman, B.S., Gross, K.W., Miner, J.H., Pippin, J.W., and Shankland, S.J. (2018). Detection of renin lineage cell transdifferentiation to podocytes in the kidney glomerulus with dual lineage tracing. *Kidney Int.* 93, 1240–1246. <https://doi.org/10.1016/j.kint.2018.01.014>.
- Fan, Y., Sun, Y., Chang, W., Zhang, X., Tang, J., Zhang, L., and Liao, H. (2018). Bioluminescence imaging and two-photon microscopy guided laser ablation of GBM decreases tumor burden. *Theranostics* 8, 4072–4085. <https://doi.org/10.7150/thno.25357>.
- Fazekas, B., and Griffin, M.D. (2020). Mesenchymal stromal cell-based therapies for acute kidney injury: progress in the last decade. *Kidney Int.* 97, 1130–1140. <https://doi.org/10.1016/j.kint.2019.12.019>.
- Feng, G., Zhang, J., Li, Y., Nie, Y., Zhu, D., Wang, R., Liu, J., Gao, J., Liu, N., He, N., et al. (2016). IGF-1 C domain-modified hydrogel enhances cell therapy for AKI. *J. Am. Soc. Nephrol.* 27, 2357–2369. <https://doi.org/10.1681/ASN.2015050578>.
- FitzSimons, M., Beauchemin, M., Smith, A.M., Stroh, E.G., Kelsch, D.J., Lamb, M.C., Tootle, T.L., and Yin, V.P. (2020). Cardiac injury modulates critical components of prostaglandin E2 signaling during zebrafish heart regeneration. *Sci. Rep.* 10, 3095. <https://doi.org/10.1038/s41598-020-59868-6>.
- Gao, L., Zhong, X., Jin, J., Li, J., and Meng, X.M. (2020). Potential targeted therapy and diagnosis based on novel insight into growth factors, receptors, and downstream effectors in acute kidney injury and acute kidney injury-chronic kidney disease progression. *Signal Transduct. Target Ther.* 5, 9. <https://doi.org/10.1038/s41392-020-0106-1>.
- Garcia, J.R., Campbell, P.F., Kumar, G., Langberg, J.J., Cesar, L., Wang, L., Garcia, A.J., and Levit, R.D. (2017). A minimally invasive, translational method to deliver hydrogels to the heart through the pericardial space. *JACC Basic Transl. Sci.* 2, 601–609. <https://doi.org/10.1016/j.jacbt.2017.06.003>.
- Gonzalez, S.R., Cortes, A.L., Silva, R.C.D., Lowe, J., Prieto, M.C., and Silva Lara, L.D. (2019). Acute kidney injury overview: from basic findings to new prevention and therapy strategies. *Pharmacol. Ther.* 200, 1–12. <https://doi.org/10.1016/j.pharmthera.2019.04.001>.
- Hato, T., Winfree, S., Day, R., Sandoval, R.M., Molitoris, B.A., Yoder, M.C., Wiggins, R.C., Zheng, Y., Dunn, K.W., and Dagher, P.C. (2017). Two-photon intravital fluorescence lifetime imaging of the kidney reveals cell-type specific metabolic signatures. *J. Am. Soc. Nephrol.* 28, 2420–2430. <https://doi.org/10.1681/ASN.2016101153>.
- He, N., Zhang, L., Cui, J., and Li, Z. (2014). Bone marrow vascular niche: home for hematopoietic stem cells. *Bone Marrow Res.* 2014, 128436. <https://doi.org/10.1155/2014/128436>.
- Honkura, N., Richards, M., Lavina, B., Sainz-Jaspeado, M., Betsholtz, C., and Claesson-Welsh, L. (2018). Intravital imaging-based analysis tools for vessel identification and assessment of concurrent dynamic vascular events. *Nat. Commun.* 9, 2746. <https://doi.org/10.1038/s41467-018-04929-8>.
- Hsueh, Y.C., Wu, J.M., Yu, C.K., Wu, K.K., and Hsieh, P.C. (2014). Prostaglandin E2 promotes post-infarction cardiomyocyte replenishment by endogenous stem cells. *EMBO Mol. Med.* 6, 496–503. <https://doi.org/10.1002/emmm.201303687>.
- Huang, Z., Du, W., He, Z.X., and Li, Z. (2015). Molecular imaging of angiogenesis in cardiovascular diseases. *J. Mol. Biol. Mol. Imaging* 2, 1012.
- Humphreys, B.D., Cantaluppi, V., Portilla, D., Singbartl, K., Yang, L., Rosner, M.H., Kellum, J.A., Ronco, C., and Acute Dialysis Quality Initiative, X.W.G. (2016). Targeting endogenous repair pathways after AKI. *J. Am. Soc. Nephrol.* 27, 990–998. <https://doi.org/10.1681/ASN.2015030286>.
- James, M.T., Bhatt, M., Pannu, N., and Tonelli, M. (2020). Long-term outcomes of acute kidney injury and strategies for improved care. *Nat. Rev. Nephrol.* 16, 193–205. <https://doi.org/10.1038/s41581-019-0247-z>.
- Kang, H.M., Huang, S., Reidy, K., Han, S.H., Chinga, F., and Susztak, K. (2016). Sox9-Positive progenitor cells play a key role in renal tubule epithelial regeneration in mice. *Cell Rep.* 14, 861–871. <https://doi.org/10.1016/j.celrep.2015.12.071>.
- Kaverina, N.V., Eng, D.G., Freedman, B.S., Kutz, J.N., Chozinski, T.J., Vaughan, J.C., Miner, J.H., Pippin, J.W., and Shankland, S.J. (2019). Dual lineage tracing shows that glomerular parietal epithelial cells can transdifferentiate toward the adult podocyte fate. *Kidney Int.* 96, 597–611. <https://doi.org/10.1016/j.kint.2019.03.014>.
- Kim, H.B., Kim, M., Park, Y.S., Park, I., Kim, T., Yang, S.Y., Cho, C.J., Hwang, D., Jung, J.H., Markowitz, S.D., et al. (2017). Prostaglandin E2 activates YAP and a positive-signaling loop to promote colon regeneration after colitis but also carcinogenesis in mice. *Gastroenterology* 152,

- 616–630. <https://doi.org/10.1053/j.gastro.2016.11.005>.
- Kindt, N., Menzebach, A., Van de Wouwer, M., Betz, I., De Vriese, A., and Conway, E.M. (2008). Protective role of the inhibitor of apoptosis protein, survivin, in toxin-induced acute renal failure. *FASEB J.* 22, 510–521. <https://doi.org/10.1096/fj.07-8882com>.
- Kozak, K.R., Crews, B.C., Ray, J.L., Tai, H.H., Morrow, J.D., and Marnett, L.J. (2001). Metabolism of prostaglandin glycerol esters and prostaglandin ethanalamides in vitro and in vivo. *J. Biol. Chem.* 276, 36993–36998. <https://doi.org/10.1074/jbc.M105854200>.
- Kumar, S., Liu, J., Pang, P., Krautzberger, A.M., Reginensi, A., Akiyama, H., Schedl, A., Humphreys, B.D., and McMahon, A.P. (2015). Sox9 activation highlights a cellular pathway of renal repair in the acutely injured mammalian kidney. *Cell Rep.* 12, 1325–1338. <https://doi.org/10.1016/j.celrep.2015.07.034>.
- Lee, A.S., Inayathullah, M., Lijkwan, M.A., Zhao, X., Sun, W., Park, S., Hong, W.X., Parekh, M.B., Malkovskiy, A.V., Lau, E., et al. (2018). Prolonged survival of transplanted stem cells after ischaemic injury via the slow release of pro-survival peptides from a collagen matrix. *Nat. Biomed. Eng.* 2, 104–113. <https://doi.org/10.1038/s41551-018-0191-4>.
- Li, Y., Feng, J., Song, S., Li, H., Yang, H., Zhou, B., Li, Y., Yue, Z., Lian, H., Liu, L., et al. (2020). gp130 controls cardiomyocyte proliferation and heart regeneration. *Circulation* 142, 967–982. <https://doi.org/10.1161/circulationaha.119.044484>.
- Little, M.H., and Kairath, P. (2016). Regenerative medicine in kidney disease. *Kidney Int.* 90, 289–299. <https://doi.org/10.1016/j.kint.2016.03.030>.
- Liu, D., Lun, L., Huang, Q., Ning, Y., Zhang, Y., Wang, L., Yin, Z., Zhang, Y., Xia, L., Yin, Z., et al. (2018). Youthful systemic milieu alleviates renal ischemia-reperfusion injury in elderly mice. *Kidney Int.* 94, 268–279. <https://doi.org/10.1016/j.kint.2018.03.019>.
- Liu, N., Qi, X., Han, Z., Liang, L., Kong, D., Han, Z., Zhao, S., He, Z.X., and Li, Z. (2016). Bone marrow is a reservoir for cardiac resident stem cells. *Sci. Rep.* 6, 28739. <https://doi.org/10.1038/srep28739>.
- Liu, Y., Cui, J., Wang, H., Hezam, K., Zhao, X., Huang, H., Chen, S., Han, Z., Han, Z.C., Guo, Z., and Li, Z. (2020). Enhanced therapeutic effects of MSC-derived extracellular vesicles with an injectable collagen matrix for experimental acute kidney injury treatment. *Stem Cell Res. Ther.* 11, 161. <https://doi.org/10.1186/s13287-020-01668-w>.
- Liu, Y., and Li, Z. (2021). Intravital microscopy imaging of kidney injury and regeneration. *Renal Replace. Ther.* 7, 23. <https://doi.org/10.1186/s41100-021-00342-y>.
- Loforese, G., Malinka, T., Keogh, A., Baier, F., Simillion, C., Montani, M., Halazonetis, T.D., Candinas, D., and Stroka, D. (2017). Impaired liver regeneration in aged mice can be rescued by silencing Hippo core kinases MST1 and MST2. *EMBO Mol. Med.* 9, 46–60. <https://doi.org/10.15252/emmm.201506089>.
- Lumelsky, N., O’Hayre, M., Chander, P., Shum, L., and Somerman, M.J. (2018). Autotherapies: enhancing endogenous healing and regeneration. *Trends Mol. Med.* 24, 919–930. <https://doi.org/10.1016/j.molmed.2018.08.004>.
- Martinez-Colon, G.J., and Moore, B.B. (2018). Prostaglandin E2 as a regulator of immunity to pathogens. *Pharmacol. Ther.* 185, 135–146. <https://doi.org/10.1016/j.pharmthera.2017.12.008>.
- Morizane, R., and Bonventre, J.V. (2017). Kidney organoids: a translational journey. *Trends Mol. Med.* 23, 246–263. <https://doi.org/10.1016/j.molmed.2017.01.001>.
- Moya, I.M., and Halder, G. (2019). Hippo-YAP/TAZ signalling in organ regeneration and regenerative medicine. *Nat. Rev. Mol. Cell Biol.* 20, 211–226. <https://doi.org/10.1038/s41580-018-0086-y>.
- Nasrallah, R., Hassouneh, R., and Hebert, R.L. (2016). PGE2, kidney disease, and cardiovascular risk: beyond hypertension and diabetes. *J. Am. Soc. Nephrol.* 27, 666–676. <https://doi.org/10.1681/ASN.2015050528>.
- Norregaard, R., Kwon, T.H., and Frokiaer, J. (2015). Physiology and pathophysiology of cyclooxygenase-2 and prostaglandin E2 in the kidney. *Kidney Res. Clin. Pract.* 34, 194–200. <https://doi.org/10.1016/j.krcp.2015.10.004>.
- Palla, A.R., Ravichandran, M., Wang, Y.X., Alexandrova, L., Yang, A.V., Kraft, P., Holbrook, C.A., Schurch, C.M., Ho, A.T.V., and Blau, H.M. (2021). Inhibition of prostaglandin-degrading enzyme 15-PGDH rejuvenates aged muscle mass and strength. *Science* 371. <https://doi.org/10.1126/science.abc8059>.
- Rakhilin, N., Garrett, A., Eom, C.Y., Chavez, K.R., Small, D.M., Daniel, A.R., Kaelberer, M.M., Mejooli, M.A., Huang, Q., Ding, S., et al. (2019). An intravital window to image the colon in real time. *Nat. Commun.* 10, 5647. <https://doi.org/10.1038/s41467-019-13699-w>.
- Roche, K.C., Gracz, A.D., Liu, X.F., Newton, V., Akiyama, H., and Magness, S.T. (2015). SOX9 maintains reserve stem cells and preserves radioresistance in mouse small intestine. *Gastroenterology* 149, 1553–1563.e1510. <https://doi.org/10.1053/j.gastro.2015.07.004>.
- Segura-Ibarra, V., Cara, F.E., Wu, S., Iruegas-Nunez, D.A., Wang, S., Ferrari, M., Ziemys, A., Valderrabano, M., and Blanco, E. (2017). Nanoparticles administered intrapericardially enhance payload myocardial distribution and retention. *J. Control Release* 262, 18–27. <https://doi.org/10.1016/j.jconrel.2017.07.012>.
- Song, S., Ajani, J.A., Honjo, S., Maru, D.M., Chen, Q., Scott, A.W., Heallen, T.R., Xiao, L., Hofstetter, W.L., Weston, B., et al. (2014). Hippo coactivator YAP1 upregulates SOX9 and endows esophageal cancer cells with stem-like properties. *Cancer Res.* 74, 4170–4182. <https://doi.org/10.1158/0008-5472.CAN-13-3569>.
- Soranno, D.E., Rodell, C.B., Altmann, C., Duplantis, J., Andres-Hernando, A., Burdick, J.A., and Faubel, S. (2016). Delivery of interleukin-10 via injectable hydrogels improves renal outcomes and reduces systemic inflammation following ischemic acute kidney injury in mice. *Am. J. Physiol. Ren. Physiol.* 311, F362–F372. <https://doi.org/10.1152/ajprenal.00579.2015>.
- Tremblay, M., Viala, S., Shafer, M.E., Graham-Paquin, A.L., Liu, C., and Bouchard, M. (2020). Regulation of stem/progenitor cell maintenance by BMP5 in prostate homeostasis and cancer initiation. *Elife* 9, e54542. <https://doi.org/10.7554/eLife.54542>.
- van den Berg, C.W., Ritsma, L., Avramut, M.C., Wiersma, L.E., van den Berg, B.M., Leuning, D.G., Lievers, E., Koning, M., Vanslambrouck, J.M., Koster, A.J., et al. (2018). Renal subcapsular transplantation of PSC-derived kidney organoids induces neo-vasculogenesis and significant glomerular and tubular maturation in vivo. *Stem Cell Rep.* 10, 751–765. <https://doi.org/10.1016/j.stemcr.2018.01.041>.
- Wong, J.S., Meliandro, K., Ray, J., and Campbell, K.N. (2016). Hippo signaling in the kidney: the good and the bad. *Am. J. Physiol. Ren. Physiol.* 311, F241–F248. <https://doi.org/10.1152/ajprenal.00500.2015>.
- Xiao, C.Y., Yuhki, K., Hara, A., Fujino, T., Kuriyama, S., Yamada, T., Takayama, K., Takahata, O., Karibe, H., Taniguchi, T., et al. (2004). Prostaglandin E2 protects the heart from ischemia-reperfusion injury via its receptor subtype EP4. *Circulation* 109, 2462–2468. <https://doi.org/10.1161/01.CIR.0000128046.54681.97>.
- Xu, J., Li, P.X., Wu, J., Gao, Y.J., Yin, M.X., Lin, Y., Yang, M., Chen, D.P., Sun, H.P., Liu, Z.B., et al. (2016). Involvement of the Hippo pathway in regeneration and fibrogenesis after ischaemic acute kidney injury: YAP is the key effector. *Clin. Sci. (Lond)* 130, 349–363. <https://doi.org/10.1042/CS20150385>.
- Yao, X., Liu, Y., Gao, J., Yang, L., Mao, D., Stefanitsch, C., Li, Y., Zhang, J., Ou, L., Kong, D., et al. (2015). Nitric oxide releasing hydrogel enhances the therapeutic efficacy of mesenchymal stem cells for myocardial infarction. *Biomaterials* 60, 130–140. <https://doi.org/10.1016/j.biomaterials.2015.04.046>.
- Young, R.N., and Grynblas, M.D. (2018). Targeting therapeutics to bone by conjugation with bisphosphonates. *Curr. Opin. Pharmacol.* 40, 87–94. <https://doi.org/10.1016/j.coph.2018.03.010>.
- Zaiss, D.M.W., Gause, W.C., Osborne, L.C., and Artis, D. (2015). Emerging functions of amphiregulin in orchestrating immunity, inflammation, and tissue repair. *Immunity* 42, 216–226. <https://doi.org/10.1016/j.immuni.2015.01.020>.
- Zaw Thin, M., Ogunlade, O., Comenge, J., Patrick, P.S., Stuckey, D.J., David, A.L., Lythgoe, M.F., Beard, P., and Kalber, T.L. (2020). Stem cell delivery to kidney via minimally invasive ultrasound-guided renal artery injection in mice. *Sci. Rep.* 10, 7514. <https://doi.org/10.1038/s41598-020-64417-2>.
- Zhang, C., Shang, Y., Chen, X., Midgley, A.C., Wang, Z., Zhu, D., Wu, J., Chen, P., Wu, L., Wang, X., et al. (2020). Supramolecular nanofibers containing arginine-glycine-aspartate (RGD) peptides boost therapeutic efficacy of

extracellular vesicles in kidney repair. *ACS Nano* 14, 12133–12147. <https://doi.org/10.1021/acsnano.0c05681>.

Zhang, K., and Li, Z. (2020). Molecular imaging of therapeutic effect of mesenchymal stem cell-derived exosomes for Hindlimb ischemia treatment. In *Imaging and Tracking Stem Cells: Methods and Protocols*, K. Turksen, ed. (Springer), pp. 213–225. <https://doi.org/10.1007/978107150221>.

Zhang, M., Lin, Q., Qi, T., Wang, T., Chen, C.C., Riggs, A.D., and Zeng, D. (2016). Growth factors and medium hyperglycemia induce Sox9+ ductal cell differentiation into beta cells in mice with reversal of diabetes. *Proc. Natl. Acad. Sci. U S A*

113, 650–655. <https://doi.org/10.1073/pnas.1524200113>.

Zhang, S., Liu, Y., Zhang, X., Zhu, D., Qi, X., Cao, X., Fang, Y., Che, Y., Han, Z.C., He, Z.X., et al. (2018). Prostaglandin E2 hydrogel improves cutaneous wound healing via M2 macrophages polarization. *Theranostics* 8, 5348–5361. <https://doi.org/10.7150/thno.27385>.

Zhang, Y., and Daaka, Y. (2011). PGE2 promotes angiogenesis through EP4 and PKA Cgamma pathway. *Blood* 118, 5355–5364. <https://doi.org/10.1182/blood-2011-04-350587>.

Zhang, Y., Desai, A., Yang, S.Y., Bae, K.B., Antczak, M.I., Fink, S.P., Tiwari, S., Willis, J.E.,

Williams, N.S., Dawson, D.M., et al. (2015). Inhibition of the prostaglandin-degrading enzyme 15-PGDH potentiates tissue regeneration. *Science* 348, aaa2340. <https://doi.org/10.1126/science.aaa2340>.

Zhao, X., Cui, K., and Li, Z. (2019). The role of biomaterials in stem cell-based regenerative medicine. *Future Med. Chem.* 11, 1777–1790. <https://doi.org/10.4155/fmc-2018-0347>.

Zhou, X., Li, Y., Wang, W., Wang, S., Hou, J., Zhang, A., Lv, B., Gao, C., Yan, Z., Pang, D., et al. (2020). Regulation of Hippo/YAP signaling and esophageal squamous carcinoma progression by an E3 ubiquitin ligase PARK2. *Theranostics* 10, 9443–9457. <https://doi.org/10.7150/thno.46078>.

STAR★METHODS

KEY RESOURCES TABLE

REAGENT or RESOURCE	SOURCE	IDENTIFIER
<b>Antibodies</b>		
anti-Yap(H-9)	Santa Cruz Biotechnology	Cat#sc-271134; RRID: AB_10612397
anti-Phospho-YAP (Ser127)	Cell Signaling Technology	Cat#13008; RRID: AB_2650553
anti-Sox9 (D8G8H)	Abcam	Cat#ab185966; RRID: AB_2728660
anti-Ki-67(D3B5)	Cell Signaling Technology	Cat#12075; RRID: AB_2728830
anti-Kim-1	Abcam	Cat#ab47635; RRID: AB_882998
anti- $\alpha$ -SMA	BOSTER	Cat#BM0002; RRID: AB_2811044
anti-CD31	BD Biosciences Pharmingen	Cat#550274; RRID: AB_393571
anti-Areg	Abcam	Cat#ab180722
anti-Survivin(D-8)	Santa Cruz	Cat#sc-17779; RRID: AB_628302
anti-Phospho-LATS1 (Thr1079)	Cell Signaling Technology	Cat#8654; RRID: AB_10971635
anti-COL IV	Abcam	Cat#ab19808; RRID: AB_445160
anti- $\beta$ -tubulin	Proteintech Group	Cat#10068-1-AP; RRID: AB_2303998
<b>Chemicals, peptides, and recombinant proteins</b>		
PGE <sub>2</sub>	Santa Cruz	Cat#sc-201225
Collagen I, Rat Tail	Corning	Cat#354236
4-hydrazinobenzoic acid	Molbase	Cat#SJ000FFC61940
Polyethylenimine	Polysciences, Inc	Cat#19850
EDC (1-ethyl-3-[3-dimethylaminopropyl] carbodiimide hydrochloride)	Thermo Scientific	Cat#22980
sulfo-NHS(N-hydroxysulfosuccinimide)	Thermo Scientific	Cat#24510
TRizol reagent	Invitrogen	Cat#15596018
RIPA lysis buffer	Solarbio	Cat#R0010
Hieff® qPCR SYBR® Green Master Mix (No Rox)	Yeasen	Cat#11201ES08
FITC-labeled LTL	Vector Laboratories	Cat# FL-1321-2
DAPI	Beyotime Biotechnology	Cat#C1002
2-(N-morpholino) ethanesulfonic acid	Sangon Biotech	Cat#145224
<b>Biological samples</b>		
primary renal tubular epithelial cells	This Paper	N/A
Transgenic mice for C57BL/6 Rosa26 <sup>mTmG</sup> transgenic mice	Jackson Laboratory	Cat#007676
C57BL/6 Sox9-Cre <sup>ERT2</sup> transgenic mice	Jackson Laboratory	Cat#018829
C57BL/6 mice	Laboratory Animal Center of the Academy of Military Medical Science	N/A
<b>Critical commercial assays</b>		
PGE <sub>2</sub> Enzyme Immunoassay Kit	ArborAssays	Cat#K051-H1
Urea Assay Kit	Nanjing Jiancheng Bioengineering Institute	Cat#C013-1
Creatinine Assay Kit	Nanjing Jiancheng Bioengineering Institute	Cat#C011-1
Cell Counting Kit-8	Beyotime Biotechnology	Cat#C0038
Reverse transcriptase core kit	Takara	Cat#RR037A

(Continued on next page)

**Continued**

REAGENT or RESOURCE	SOURCE	IDENTIFIER
Hoechst Staining Kit	Beyotime Biotechnology	Cat#C0003
<b>Oligonucleotides</b>		
<i>Bad</i> 5'-AAGTCCGATCCCGAATCC-3'	This paper	N/A
<i>Bad</i> 5'-GCTCACTCGGCTCAAACCT-3'	This paper	N/A
<i>Bax</i> 5'-TGAAGACAGGGCCTTTTG-3'	This paper	N/A
<i>Bax</i> 5'-AATTCGCCGAGACTCG-3'	This paper	N/A
<i>Caspase3</i> 5'-TGGTGATGAAGGGTC ATTTATG-3'	This paper	N/A
<i>Caspase3</i> 5'-TTCGGCTTCCAGTCAGA CTC-3'	This paper	N/A
<i>Fas</i> 5'-TATCAAGGAGGCCATTTGTC-3'	This paper	N/A
<i>Fas</i> 5'-TGTTTCCACTTCTAAACCATGCT-3'	This paper	N/A
<i>Gapdh</i> 5'-AGGTCGGTGTGAACGGATTG-3'	This paper	N/A
<i>Gapdh</i> 5'-TGTAGACCATGTAGTTGAGG TCA-3'	This paper	N/A
<i>Nonspecific shRNA (sh Ctrl)</i> 5'-CCGG-CA ACAAGATGAAGAGCACCAA-CTCGAG- TTGGTGCTTTCATCTTGTG-TTTTGG-3'	Sigma-Aldrich	Cat#SHC002
<i>shRNA-Yap (sh Yap)</i> 5'-CCGG-GCAGAC AGATTCCTTTGTAA-CTCGAG-TTAAC AAAGGAATCTGTCTGC-TTTTGG-3'	Broad Institute	TRCN0000095864
<b>Software and algorithms</b>		
Two-photon microscope system	Olympus	FV1000
Scanning electron microscopy (SEM)	HITACHI	X-650
FT-IR spectromete	Bio-Rad	FTS-6000
Parallel-plate rheometer	New Castle	N/A
Imaris	Oxinst	<a href="https://imaris.oxinst.com/">https://imaris.oxinst.com/</a>
Prism 8	GraphPad	<a href="https://www.graphpad.com/scientific-software/prism/">https://www.graphpad.com/scientific-software/prism/</a>
ImageJ	ImageJ	<a href="https://imagej.nih.gov/ij">https://imagej.nih.gov/ij</a>

**RESOURCE AVAILABILITY**

**Lead contact**

Further information, inquiries, and request should be directed to the lead contact Zongjin Li ([zongjinli@nankai.edu.cn](mailto:zongjinli@nankai.edu.cn)).

**Materials availability**

All requests for resources and reagents should be directed to and will be fulfilled by the lead contact Zongjin Li ([zongjinli@nankai.edu.cn](mailto:zongjinli@nankai.edu.cn)). All reagents will be made available on request after completion of a Materials Transfer Agreement.

**Data and code availability**

Any additional information required to reanalyze the data reported in this paper is available from the lead contact upon request.

No original code was produced in this study.

## EXPERIMENTAL MODEL AND SUBJECT DETAILS

### AKI model and COL-PGE<sub>2</sub> matrix delivery

Adult male wild-type C57BL/6 mice (7-8 weeks old, weight 25-30 g) were purchased from the Laboratory Animal Center of the Academy of Military Medical Sciences (Beijing, China). Animals were randomly assigned to six groups according to the complete randomization method, and each group included five single mice. An AKI model induced by ischemia/perfusion was established as previously described (Liu et al., 2018). Briefly, the animals were anesthetized by intraperitoneal injection of 2.5% avertin (Sigma-Aldrich) at a dose of 240 mg/kg. Mice were clamped to the left kidney pedicle for 40 min followed by removal of the right kidney after injury. Reperfusion was visually confirmed before delivery of the matrix. After 10 min of reperfusion, 75  $\mu$ l of PBS, COL, PGE<sub>2</sub>/COL or COL-PGE<sub>2</sub> matrix was injected into the renal capsule or the renal cortex with an insulin syringe. The kidney was kept moist with warm sterile saline prior to delivery of the matrix. The needle of the matrix-containing syringe pierced the kidney capsule at the upper end of the kidney. The needle was slowly moved from the upper end to the lower end along the inner surface of the renal capsule. The middle of the needle was pressed to slowly inject the matrix; then, the syringe was slowly pulled out and the injection site was pressed with a cotton swab for 3-5 min. The kidney was returned to the abdominal cavity after the matrix solidified and the wound was sewn. The animal was placed in an incubator until it came out from anesthesia. In addition, another group of intra-local injections of COL-PGE<sub>2</sub> matrix was administered as the control group. Injection of PBS and collagen matrix was performed in controls. Sham-operated animals were subjected to the same surgical procedure without renal ischemia or matrix injection. The treatment of animals and the experimental procedures of the present study adhere to the Nankai University Animal Care and Use Committee Guidelines (approval no. IRM-DWLL-2019121), which is in accordance with the Guidelines for Animal Care Guidelines approved by the National Institutes of Health (NIH).

### Tracing of the Sox9 lineage with transgenic mice

Male C57BL/6 Sox9-Cre<sup>ERT2</sup>; Rosa26<sup>mTmG</sup> transgenic mice were purchased from Jackson Laboratory (Jax strains: 007676 and 018829) and have been used for lineage tracing in multiple studies (Balani et al., 2017; Roche et al., 2015; Zhang and Li, 2020; Zhang et al., 2016). Mice were randomly divided into 6 groups at random and each group included 3 single mice. Rosa26<sup>mTmG</sup> mice express the fluorescent protein tdTomato (red) under the  $\beta$ -actin promoter. Through Cre-mediated recombination, the Tomato and STOP codons are excised, and EGFP is expressed in these animals. Sox9-Cre<sup>ERT2</sup> animals express a ligand-dependent chimeric Cre recombinase under the Sox9 promoter. Cell labeling occurs only at the time of tamoxifen injection, but daughter cells retain the labels, as genetic recombination cannot be reversed in the nucleus. EGFP is expressed in a Sox9<sup>+</sup> cell type-specific manner. Transgenic mice were identified by genomic PCR analysis. Only 5- to 8-week-old male mice were used in the study. Mice were injected with tamoxifen dissolved in corn oil intraperitoneally (100 mg/kg daily, mice were injected 3 times a week before the experiment).

## METHOD DETAILS

### Preparation of the COL-PGE<sub>2</sub> matrix

As summarized in Figure 1A, PGE<sub>2</sub> was first linked to the PEI-HBA cross-linker to obtain PEI-HBA-PGE<sub>2</sub> conjugates, and then the PEI-HBA-PGE<sub>2</sub> conjugates were further covalently cross-linked to collagen through dehydration condensation. In detail, to increase/decrease, 4.8  $\mu$ mol branched polyethylenimine (PEI, Mw = 10000, 60 mg) and 0.1 mmol of 4-hydrazinobenzoic acid (HBA, 14.8 mg) were dissolved in 5 mL of dimethyl sulfoxide (DMSO), and then 0.28 mmol 1-(3-dimethylaminopropyl)-3-ethylcarbodiimide hydrochloride (EDC, 54 mg) and 0.28 mmol N-hydroxy-succinimide (sulfo-NHS, 32 mg) were added. The mixture was stirred for 24 h at room temperature in an atmosphere of nitrogen and then the HBA-PEI conjugates were dialyzed against H<sub>2</sub>O to remove unreacted HBA (molecular weight cutoff [MWCO] = 3,500) and lyophilized to obtain a fine powder for the next step (Figure S1A). For the cross-linking of PGE<sub>2</sub>, the PGE<sub>2</sub> (10 mg, CAS 363-24-6; Santa Cruz Biotechnology) and PEI-HBA conjugates (30 mg) were dissolved separately in 10 mL of ethanol and mixed together, and the mixture was added to 2 mL of glacial acetic acid, stirred for 2 h. The reaction mixture was heated to 80°C, refluxed by adding molecular sieves under nitrogen for 20 h, and allowed to cool at 0°C. The product was dialyzed against H<sub>2</sub>O (MWCO = 3,500) and lyophilized to obtain a fine powder (HBA-PEI-PGE<sub>2</sub>) (Figure S1B). The last step was to link the HBA-PEI-PGE<sub>2</sub> conjugates to collagen (Figure S1C). To activate collagen, 5 mg of EDC and 5 mg of sulfo-NHS were added to 6 mL of collagen solution, which was dialysed against 2-(N-morpholino) ethanesulfonic acid (MES buffer,

50 mM) and reacted for 20 min at room temperature, and then 1.4  $\mu\text{L}$  of 2-mercaptoethanol (final concentration 20 mM) was added to quench EDC. The activated collagen was separated from the excess reducing agent and the inactivated cross-linker using Ultra-4 Centrifugal Filter Units (100 kDa), and the collagen was rinsed with 3 mL MES buffer (pH 7.0, 50 mM). The activated collagen was mixed with the HBA-PEI-PGE<sub>2</sub> conjugates and allowed to react overnight with stirring at 4°C, and then was ultrafiltered and washed with sterile H<sub>2</sub>O to remove the unreacted conjugates and cross-linking reagents by using Ultra-4 Centrifugal Filter Units (100 kDa) at 4°C. Collagen was collected in PBS and then freeze-dried to yield the final product (COL-PGE<sub>2</sub>).

### Characterization of the COL-PGE<sub>2</sub> matrix

The morphology of the COL, PGE<sub>2</sub>/COL and COL-PGE<sub>2</sub> matrix was assessed by scanning electron microscopy (SEM; HITACHI X-650, Tokyo, Japan). The chemical structures of the COL, PGE<sub>2</sub>/COL and COL-PGE<sub>2</sub> matrices were characterized using FT-IR. The FT-IR transmittance spectrum in the wavelength region from 4000 to 400  $\text{cm}^{-1}$  was acquired using an FT-IR spectrometer (FTS-6000 spectrometer; Bio-Rad, Hercules, CA). Furthermore, the rheological properties of the COL, PGE<sub>2</sub>/COL and PGE<sub>2</sub> matrices were measured on a 25-mm parallel-plate rheometer (TA Instruments, New Castle, DE) as previously reported. In summary, the elastic moduli ( $G'$ ) and the viscous moduli ( $G''$ ) of the COL, PGE<sub>2</sub>/COL and COL-PGE<sub>2</sub> matrices at different temperatures from 4°C to 42°C were measured at a frequency of 0.159 Hz. The rheologic properties of the samples were measured within a temperature range of 4°C–42°C with a constant heating rate of 2°C/min. The changes in the elastic (storage) modulus ( $G'$ ) and the viscous (loss) modulus ( $G''$ ) were recorded as the change in temperature at a fixed frequency of 1 rad/s. The phase lag ( $\delta$ ) was used to determine the gelation temperature at which the elastic modulus ( $G'$ ) and the viscous modulus ( $G''$ ) were equivalent.

### Biocompatibility of the COL-PGE<sub>2</sub> matrix

To determine the optimal concentration of the COL-PGE<sub>2</sub> matrix for pRTEC proliferation, a cell counting kit-8 assay was used to detect cell proliferation of cells cultured in 96-well plates coated with no coating, collagen-coated, PGE<sub>2</sub>/COL coated or COL-PGE<sub>2</sub> matrix-coated 96-well plates for 48 h and 72 h. To investigate the biocompatibility of the COL-PGE<sub>2</sub> matrix, 96-well plates were coated with collagen, PGE<sub>2</sub>/COL or COL-PGE<sub>2</sub> matrix and  $1 \times 10^4$  pRTECs were added per well. Cell viability was assessed using Trypan blue cell counting with Trypan blue. Cell viability was calculated and normalized according to the initial viability of the culture.

### Measurement of PGE<sub>2</sub> release

For the *in vitro* PGE<sub>2</sub> release assay, 200  $\mu\text{L}$  of the COL/PGE<sub>2</sub> matrix and the COL-PGE<sub>2</sub> matrix were deposited at the bottom of a 1.5 mL test tube, incubated at 37°C for 15 min, and covered with a layer of  $1 \times$  PBS buffer. Two hundred microliters of collagen that was cross-linked with PGE<sub>2</sub> or was not cross-linked was deposited at the bottom of a 1.5 mL microcentrifuge tube. After incubation at 37°C for 15 min, 500  $\mu\text{L}$  of  $1 \times$  PBS was carefully layered on top of collagen. The mixture was then incubated at 37°C for up to 16 days. One hundred microliters of solution were removed from the PBS layer at different time points and replaced with 100  $\mu\text{L}$  of fresh  $1 \times$  PBS. PGE<sub>2</sub> was measured by a chemiluminescence enzyme immunoassay (K051-H1, Assay Design, Inc., Ann Arbor, MI).

For the *in vivo* PGE<sub>2</sub> release assay, 75  $\mu\text{L}$  of COL, PGE<sub>2</sub>/COL, and COL-PGE<sub>2</sub> matrix were transplanted into the renal capsule of C57BL/6 mice (7–8 weeks old, weight 25–30 g) after AKI. Mice were anesthetized with avertin at the indicated time points (days 1, 2, 3, 7, and 14) by intraperitoneal injection. The kidney was then explanted by removing the kidney capsule and matrix, snap frozen in liquid nitrogen, and stored at –80°C until needed. To prepare kidney homogenates, tissue samples were weighed and homogenized in 50 mM Tris buffer, pH 7.5, containing antioxidant butylated hydroxytoluene (10  $\mu\text{M}$ ) and the cyclooxygenase inhibitor indomethacin (10  $\mu\text{g}/\text{mL}$ ) to block *ex vivo* arachidonic acid autooxidation and prostaglandin formation and kept on ice. The homogenates were vigorously vortexed and incubated for 5 min on ice before centrifugation at 14,000 rpm for 45 min. The supernatants were collected and stored at –80°C until needed. PGE<sub>2</sub> was measured by a chemiluminescence enzyme immunoassay (K051-H1, Assay Design, Inc., Ann Arbor, MI).

### Cell apoptosis assay

To test the cytoprotective effects of the COL-PGE<sub>2</sub> matrix,  $1 \times 10^6$  pRTECs were seeded in 6-well plates coated with non-coated COL, PGE<sub>2</sub>/COL, or COL-PGE<sub>2</sub> matrix or cultured for 24 h. Cells were then exposed to 150  $\mu$ M H<sub>2</sub>O<sub>2</sub> for 6 h. Cells in medium without H<sub>2</sub>O<sub>2</sub> served as a control. After staining with an Apoptosis Hoechst staining kit (C0003, Beyotime Biotechnology, China) for 10 min, Trizol (Invitrogen, Grand Island, NY) was added for the next step of RNA extraction. After Hoechst staining, the cells were washed with PBS to remove the remaining Hoechst 33342 and observed under a fluorescence microscope (Nikon). Apoptotic cells stained with Hoechst 33342 dye were counted, as they were distinguished by bright blue nuclear staining. The mean fluorescence intensity of the images in seven random fields of view was quantified by ImageJ software (NIH, Bethesda, Maryland).

### Knockdown of Yap in primary renal tubular epithelial cells

The shRNA (short hairpin RNA) sequences targeting Yap were individually inserted into the PLKO.1 construct. As a negative control, the nonspecific control shRNA (sh Ctrl) was inserted into the construct. Cloning was confirmed by DNA sequencing. To generate lentivirus, the shRNA construct was transfected into HEK-293T cells along with the lentivirus package constructs, pMD2.G and PAX, and allowed to incubate for 16 h. The cells were then transferred to the complete medium and cultured for an additional 24 h. The medium was harvested and concentrated. For infection, virus was added to pRTECs in polybrene (8  $\mu$ g/mL)-containing medium for 24 h. Subsequently, the medium was removed and replaced with a complete medium containing 1  $\mu$ g/mL puromycin for 3 days. The expressions of the Yap protein in stable cells were verified by Western blot assays and immunofluorescence staining.

### Intravital two-photon imaging in mice

An AIW was implanted in the abdomen of the mouse, fixed with an adapter, and maintained under anesthesia by injecting avertin. The objective lens was 25 $\times$  and immersed in water on the AIW window in the abdomen of the mouse. Two-photon excitation was performed at a wavelength of 835 nm (10% laser transmissivity), and emission was collected at 495–540 nm (EGFP) and 575–630 nm (td Tomato). Scanning was advanced with Z steps of 5  $\mu$ m and zoom under the 25 $\times$  objective lens (580  $\mu$ m  $\times$  580  $\mu$ m single scanning area) and an 800  $\times$  800-pixel size.

### Renal function analysis

For the assessment of renal function, at different time points after injury, blood samples were taken and serum was collected for the assessment of BUN and creatinine using the Colorimetric Detection Kit of Urea Nitrogen (BUN) Colorimetric Detection Kit (C013-1, Nanjing Jiancheng Institute of Bioengineering) and the Creatinine Assay Kit (C011, Nanjing Jiancheng Institute of Bioengineering).

### Histological analysis of renal tissues

At the indicated time points, the animals were sacrificed to harvest kidney samples. For paraffin sections, kidney samples were fixed with 4% paraformaldehyde, dehydrated with ethyl alcohol, hyalinized with xylene, and eventually embedded in paraffin (Leica Microsystems, Wetzlar, Germany). For cryosection, kidney samples were fixed with 4% paraformaldehyde, dehydrated with a 30% sucrose solution and embedded in Optimal Cutting Temperature (OCT) compound (Sakura Finetek, Tokyo, Japan). All samples were cut into a series of sections with a thickness of 5  $\mu$ m. Hematoxylin and eosin (H&E) staining and Masson trichrome staining were performed on paraffin sections according to a standard protocol, while frozen sections were used for immunofluorescent staining. Quantitative immunostaining analysis was performed with ImageJ software. Histological examinations were performed by three blinded renal pathologists. Histological changes caused by tubular necrosis were quantified by calculating the percent of tubules that exhibited cast formation, loss of the brush border, tubular cell necrosis as follows: 0, none; 1, 10%; 2, 11% to 25%; 3, 26% to 45%; 4, 46% to 75%; and 5, >76%. At least 10 nonoverlapping visual fields ( $\times 200$ ) were reviewed for each kidney in the HE stained specimens. Analyzes were performed blindly to treatment assignments in all experiments.

### Western blot analysis

Cells were lysed on ice in radioimmunoprecipitation assay (RIPA) buffer (Solarbio, Shanghai, China), and total protein was quantified using a BCA Protein Assay Kit (Thermo Scientific). For tissue protein analysis, renal capsules and matrix were removed from mouse kidney tissue, cut into a 1.5 mL EP tube supplemented

with a proteinase inhibitor cocktail (Sigma-Aldrich) and transferred to a homogenizer. The tissue homogenates were lysed on ice with RIPA buffer for 30 min. Total proteins were diluted in 4× SDS-PAGE loading buffer and boiled for 5 min. The harvested proteins were separated by 10% SDS-PAGE and transferred to polyvinylidene fluoride membranes (PVDF; Millipore, Darmstadt, Germany). After blocking with 5% non-fat milk for 2 h, the PVDF membranes were incubated with primary antibodies overnight at 4°C and then for 2 h at room temperature with secondary antibodies. Primary antibodies included β-tubulin (1:1000, 10068-1-AP, Proteintech Group, Wuhan, China), YAP (sc-271134, 1:500, Santa Cruz Biotechnology, CA), p-YAP (13008, 1:1000, Cell Signaling Technology, MA, USA), Arge (ab180722, 1:1000, Abcam), survivin (sc-17779, 1:500, Santa Cruz Biotechnology, CA), Sox9 (ab185966, 1:1000, Abcam), p-Lats1 (8654, 1:1000, Cell Signaling Technology, MA, USA); β-tubulin was used as an internal control.

### Quantitative real-time PCR

Total RNA was isolated from cells or tissues using TRIzol reagent (Invitrogen, Grand Island, NY) and purified using RNeasy columns (Qiagen, Chatsworth, CA). First-strand cDNA was synthesized by reverse transcriptase (TransGen Biotech, China) using oligodT primers. Subsequently, the Hieff qPCR SYBR Green Master Mix Kit (Yeasen, China) was used to quantify mRNA expression levels in 20 μl reaction volumes. Real-time PCR analysis was performed on the Opticon® System (Bio-Rad, Hercules, CA). The  $2^{-\Delta\Delta C_t}$  method was used to analyze relative gene expression. The sequences of the primers are listed in the [Key resources table](#).

### QUANTIFICATION AND STATISTICAL ANALYSIS

All presented results were obtained from at least three independent experiments for each condition. Statistical analyzes were performed using GraphPad Prism software (GraphPad Software Inc., San Diego, CA). One-way repeated measures ANOVA with Tukey post hoc tests, two-way MANOVA with Tukey post hoc tests, and two-way repeated measures ANOVA with Sidak's post hoc test were used. Differences were considered significant at a *P* value < 0.05. The analyzes were performed blindly in all experiments.

### ADDITIONAL RESOURCES

None.